Ocean Modelling 200 (2026) 102660

Contents lists available at ScienceDirect

Ocean Modelling

journal homepage: www.elsevier.com/locate/ocemod

Assessing basin scale modelling for projecting storm surge extremes under climate change scenarios in northwest Ireland

Tasneem Ahmed [a,*], Andrea Cucco [b,*], Giovanni Quattrocchi [b], Leo Creedon [c], Iulia Anton [a], Michele Bendoni [d], Stefano Taddei [e], Carlo Brandini [d], Salem S Gharbia [a]

[a] Department of Environmental Science, Atlantic Technological University, Sligo, Ireland
[b] CNR, Institute for the Study of Anthropic Impacts and Sustainability in the Marine Environment (CNR-IAS), Oristano, Italy
[c] Centre for Mathematical Modelling and Intelligent Systems for Health and Environment (MISHE), Atlantic Technological University, Sligo, Ireland
[d] CNR, Institute for the Marine Science (CNR-ISMAR), Lerici, SP, Italy
[e] LAMMA, Florence, Italy

ARTICLE INFO

Keywords:
Numerical modelling
Storm surge extremes
Extreme value analysis
Climatological statistics
Climate change
Finite element ocean model

ABSTRACT

This study evaluates the performance of the SHYFEM (System of HydrodYnamic Finite Element Modules) ocean model in simulating storm surges within Donegal Bay (northwest Ireland) for climate projection applications. A high-resolution Basin Scale Model (BSM) configuration of SHYFEM, spanning the North Atlantic is employed in barotropic mode accounting exclusively for atmospheric forcing with no tidal contribution included. To evaluate its accuracy, the BSM is compared against a Limited Area Model (LAM) configuration of SHYFEM implemented at the same study site.

The LAM includes tidal constituents through the downscaling of sea surface height (SSH) from a calibrated deep-water ocean model provided by the Copernicus Marine Environment Monitoring Service (CMEMS). Comparison is performed to quantify the impact of non-linear tide-surge interaction on residual water levels computation.

On average the LAM achieves 3 cm greater accuracy than the BSM in reproducing the time series of residual water levels measured by four tide gauges within the bay. Nevertheless, although both models tend to underestimate the extreme values, the BSM better captures the climatological statistics of storm surge events, closely matching the observed return levels associated with 5, 10, 25, and 50 year return periods.

Further improvements in return level estimates and residual water level error metrics are obtained through iterative calibration of main model parameters, validating the BSM's effectiveness in simulating storm surges despite the absence of tide-surge interaction.

A Chi-squared significance test applied to tide gauge observations confirms that tide-surge interaction is statistically non-significant within Donegal Bay for surge thresholds at the 99th, 99.95th, and 99.99th percentiles. These findings support the use of BSM, driven exclusively with atmospheric fields (without including tides), for reliable simulation of storm surges and their climatological statistics in this region.

1. Introduction

A storm surge can be described as a potentially devastating rise in the sea surface caused by extratropical or tropical cyclones (Resio and Westerink, 2008), as a result of wind driven water circulation towards or away from the coast and the inverse barometer effect (WMO, 2011). The magnitude of a storm surge is dictated by several factors like the nearshore local bathymetry (WMO, 2011), the shape of the coastline (Arns et al., 2015), the size, track, speed, and intensity of the storm system, the stratification of the water body, presence or absence of ice and the nature of tidal motion (WMO, 2011; Vousdoukas et al., 2016). Some of the worst damage to life and economy has been caused by storm surge flooding causing extreme sea levels (ESLs), thus being one of the main drivers of coastal hazard (Fernández-Montblanc et al., 2019). In a warming climate the hazard of storm surge flooding is expected to increase due to rising sea levels and changes in storm activity with local conditions dictating the combination of these two factors (Rahmstorf, 2017). Numerical models are a useful tool for better understanding

* Corresponding authors.
E-mail addresses: tasneem.ahmed@research.atu.ie (T. Ahmed), andrea.cucco@cnr.it (A. Cucco).

https://doi.org/10.1016/j.ocemod.2025.102660
Received 3 November 2024; Received in revised form 4 October 2025; Accepted 2 December 2025
Available online 3 December 2025

storm surges and for projecting their future changes under different climate scenarios as they can simulate surges with a high spatial resolution even for ungauged locations following proper model calibration and validation (Calafat et al., 2014). Several studies have been conducted on the dynamics of storm surges in Europe using the outputs of numerical models (Wang et al., 2008; Brown et al., 2010a; Mel et al., 2013; Cid et al., 2016; Vousdoukas et al., 2016).

Calafat et al. (2014) states that good model performance in simulating the observed distribution of extremes like return levels (Howard, 2022) does not necessarily translate into good predictive capability. This implies that the model may correctly simulate the main statistical properties of the extremes, but it may fail to predict their timing and magnitude as for predictive purposes like storm surge forecasting. Nevertheless, an accurate representation of the extreme value distribution may be sufficient when the focus is limited to the climatological characteristics of the extremes, as in the present study; however, such approach, may not be adequate for operational storm surge forecasting (Calafat et al., 2014). Since the primary focus of the present study is to assess the capability of the storm surge model for projecting future surge events, its ability to reproduce the statistical features of the observed sea level extremes is considered sufficient, without addressing its skill in predicting the timing of individual storm surge events. Proper validation of such numerical models is a pre-requisite prior to their utilisation for such purposes. Climatological statistical quantities like return levels can be derived from tide gauge records (Haigh et al., 2010), given that such records are of sufficient length, preferably of minimum duration of around 30 years (Macpherson et al., 2022). However, for data sparse regions like the northwest of Ireland where tide gauge records only begin around 2007, the use of numerical models is essential for reconstructing historical time series of extreme sea levels and for computing climatological statistics, following appropriate calibration and validation procedure.

Despite significant advances in storm surge modelling, there remains a notable gap in high-resolution numerical simulations focused on projecting storm surges and their associated climatological statistics (e.g., return levels) under future climate scenarios for the northwest coast of Ireland, including Donegal Bay (Laino and Iglesias, 2024b), one of the largest bays in Ireland. Due to its exposure to the North Atlantic, Donegal Bay experiences a high tidal range, making storm surges a significant threat for coastal flooding risks, particularly when they coincide with high tides (Williams et al., 2016). This limited availability of observational data in this region (OPW, 2020) has posed challenges for accurately modelling storm surges in previous studies which has been conducted using coarse-resolution numerical models without rigorous validation of the outputs with observed data (Wang et al., 2008; Olbert and Hartnett, 2010; Olbert et al., 2013). With existing studies being predominantly focused on more extensively monitored areas (Elsäßer, 2010), the northwest coast of Ireland remains relatively under-explored. Wang et al. (2008) in their study on the impact of climate change on storm surges over Irish waters found that storm surges in the range 0.5–1.0 m were projected to increase by ~25 % within the bay under future climate scenarios. Such results have important implications as the increase in storm surge magnitudes would increase the associated risk of ESL driven coastal floods. That study however was conducted using a coarse-resolution numerical model without detailed validation of the outputs with observed data for the northwest coast. For proper characterisation of future flooding risk due to ESL (combination of storm surges, high tides and mean sea level rise) in this region, this research focusses on the storm surge component of ESL, i.e., on developing a high-resolution rigorously validated numerical model capable of accurately projecting storm surges and their climatological statistics under future climate scenarios, a current research gap for this region. Addressing this gap is essential for developing effective coastal management strategies and enhancing the resilience of vulnerable communities (Laino and Iglesias, 2024b). Within the EU project SCORE (Smart control of the climate resilience in European coastal cities), this region is a coastal city living lab (Laino and Iglesias, 2024a) and has been identified as vulnerable to climate driven coastal hazards including ESL driven coastal flooding and erosion (Tiwari et al., 2025). This vulnerability underscores the need for detailed hydrodynamics of the bay, with particular emphasis on storm surges and their projected evolution under future climate scenarios.

In this context, this study aims to evaluate the capability of a finite element ocean model called System of HydrodYnamic Finite Element Modules (SHYFEM; Umgiesser et al., 2004) running in barotropic mode, to simulate storm surges in Donegal Bay and to examine its suitability for projecting future extreme events under different climate scenarios. This goal is pursued by assessing the extent to which statistical properties of model outputs agree with those from observed sea levels (Tsimplis and Blackman, 1997; Bernier et al., 2007; Marcos et al., 2009; Conte and Lionello, 2013), using quantile-quantile (Q-Q) plots to highlight similarities and differences between the modelled and observed probability distributions and assessing the model's ability to capture key climatological statistics, such as return levels using extreme value statistics (Coles, 2001).

Specifically, a high-resolution Basin Scale Model (BSM) configuration covering the entire North Atlantic, forced exclusively by atmospheric fields (10 m winds and mean sea level pressure) is used to simulate storm surges in Donegal Bay. This setup aligns with best practices in storm surge modelling worldwide whereby a large oceanic basin is exclusively forced with atmospheric fields to simulate the meteorological contribution to the sea level (residual water levels) without the inclusion of tides for both hindcasts and climate projection applications (Greatbatch et al., 1996; Ratsimandresey et al., 2008; Marcos et al., 2011, 2012; Lionello et al., 2012; Mel et al., 2013; Conte and Lionello, 2013; Calafat et al., 2014; Androulidakis et al., 2015; Vousdoukas et al., 2016; Zhang and Li, 2019; Kim et al., 2021; Antony et al., 2022; Pavlova et al., 2022; Kirstensen et al., 2024). Tidal boundary conditions are excluded based on the well-known problem of simulating correct tidal phases and amplitudes in numerical models (Kirstensen et al., 2024). However, Donegal Bay exposed to the Atlantic has a large tidal range (see Section 2.1), necessitating an assessment of the implications of excluding tide-surge interaction. For this purpose a Limited Area Model (LAM) configuration of SHYFEM, with a much smaller domain confined to the bay is employed to downscale calibrated sea surface height (SSH) data containing tidal constituents from a deep-water ocean model from CMEMS (Copernicus Marine Service, 2020) and compare the outputs, i.e., residual water level time series and storm surge return levels with the BSM. This modelling approach is imperative for quantifying any errors in the modelled storm surges in the study area using the BSM due to the non-inclusion of the tides. Such limited area models are employed frequently for computational feasibility and to represent complicated coastlines and inland waterways efficiently (Park et al., 2022). These LAMs, however, are not a suitable candidate for storm surge projection studies under future climate scenarios due to two reasons. Firstly, unlike the BSM the limited domain size truncates the wind fetch leading to underestimation in the surge response when exclusively driven by atmospheric forcings (Blain et al., 1994; Morey et al., 2006; Kerr et al., 2013; Liao and Kaihatu, 2016), and secondly, to mitigate the inadequately reproduced surge due to the atmospheric forcing alone it requires suitable open boundary conditions (OBCs; Liao and Kaihatu, 2016), i.e., SSH with the required spatio-temporal resolution for resolving the storm surges. However, the available climate models provide SSH data at monthly frequency (Sardana et al., 2024) which is insufficient to resolve storm surge signals. Atmospheric forcings from the climate models are available at a much higher temporal frequency (hourly) making BSMs more suitable for projecting storm surges under future climate scenarios (Vousdoukas et al., 2016).

Accordingly, this modelling study addresses two primary research objectives: (1) to evaluate the capability of the Basin Scale Model (BSM) approach in reproducing the climatological statistics of observed storm

surges derived from tide gauge records, thereby assessing its suitability for projecting future storm surges under climate scenarios; and (2) to compare the performance of the BSM with the locally applied SHYFEM configuration (LAM) for quantifying tide-surge interactions within the bay.

This paper is organized as follows: Section 2 provides an overview of the study site, including its tidal regime and available tide gauge observations used for model calibration and validation. Additionally, it describes the model setup, and the statistical tools applied for model evaluation. Section 3 presents the detailed results obtained from the adopted modelling approach, Section 4 discusses the results, while Section 5 concludes the paper and outlines the next steps in the research.

2. Data and methods

2.1. Site description and observations

Donegal Bay (Fig. 1), located on the northwest coast of Ireland, is one of the largest bays in Ireland, and is a prominent semi-enclosed marine embayment characterized by its intricate coastal morphology and diverse bathymetric features. The bay opens into the North Atlantic Ocean and is exposed to dominant westerly winds and oceanic swells.

The bathymetry of Donegal Bay is notably variable, ranging from shallow nearshore areas with depths shallower than 10 m to deep oceanic channels, with depths exceeding 2700 m toward the western boundary beyond the continental shelf. These bathymetric features play a crucial role in influencing tidal currents, wave dynamics, and storm surge behaviour within the region.

Four tide gauge stations (Sligo, Killybegs, Ballyglass, and Aranmore) are strategically positioned within Donegal Bay to monitor sea level (see Fig. 1), which have been used for model calibration and validation. Collectively these gauges started recording the sea level from 2007–2008 with a temporal frequency of 5 mins (also 6 mins for the earliest years when these gauges began recording) with several gaps within the records (see Figure A2 in the Appendix).

Corresponding residual water levels were extracted from the measured sea level using harmonic analysis. The package called OCE in the R programming language (Kelley, 2018; R Core Team, 2023) was

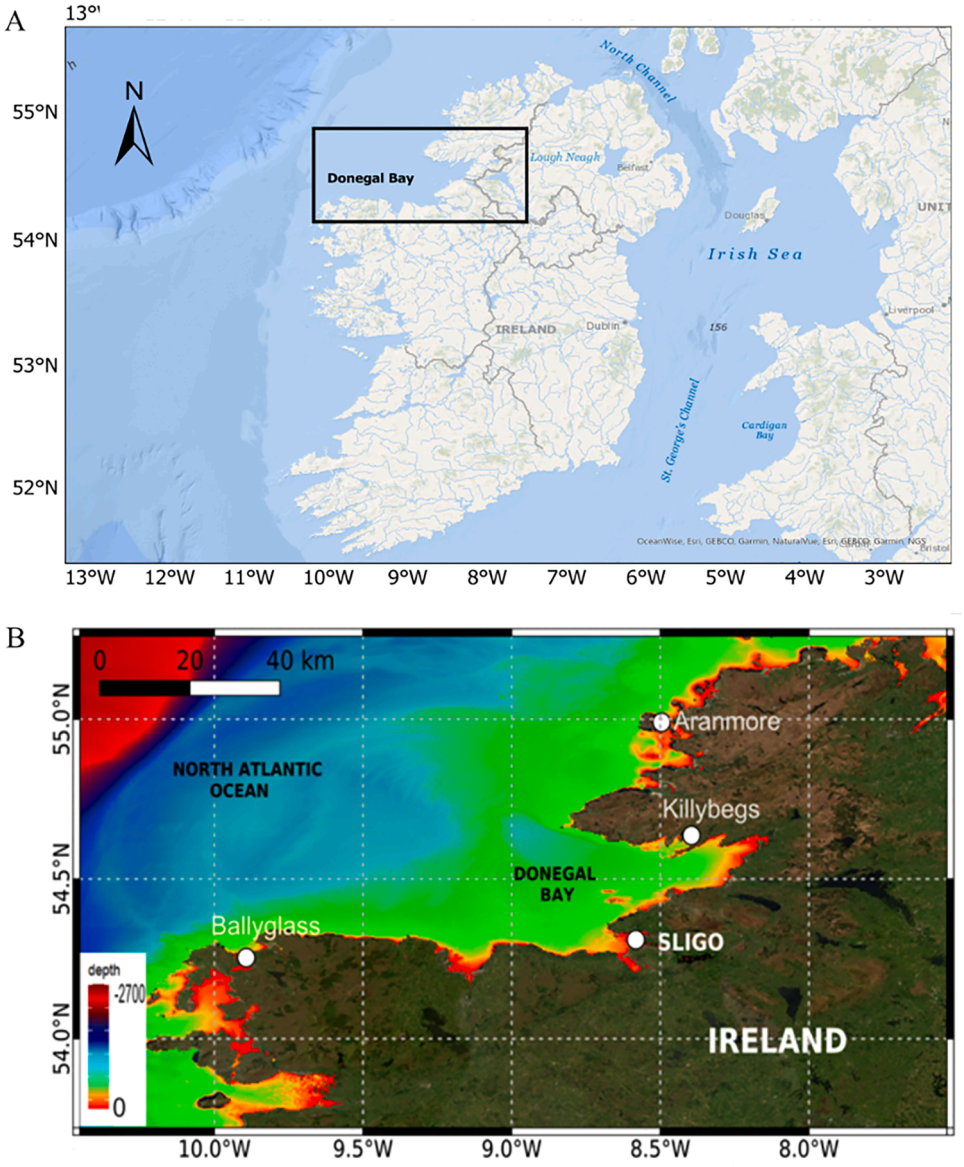

Fig. 1. (A) Map of Ireland highlighting the location of Donegal Bay, enclosed within a rectangular box. (B) Detailed bathymetric map of Donegal Bay with the location of the tide gauges shown as white dots (the bathymetry is taken from GEBCO (GEBCO, 2022).

utilised for this purpose.

The oceanographic regime of Donegal Bay is influenced by a combination of tidal and non-tidal processes. The tidal regime is semi-diurnal, with two high and two low tides each day, and a mean tidal range of about 2–4 m, with spring tides ranging between 3.5–4.5 m which can be categorised as mesotidal (Cooper et al., 2004). The interaction between the Atlantic swells and the local tidal currents contributes to the bay's dynamic water levels (Cooper et al., 2004). Naturally, the tides within the bay are influenced by the tides in the North Atlantic which, being strongly semi-diurnal, can be described by the principal semi-diurnal lunar (M2) and solar (S2) constituents and has a form factor (F) that lies within the range $0 \leq F \leq 0.25$ (Stephenson, 2017).

2.2. The SHYFEM numerical model

SHYFEM has been extensively used to reproduce water circulation and hydrodynamics in coastal and shallow water areas worldwide (Umgiesser et al., 2004, 2021; Cucco and Umgiesser, 2006; Bajo et al., 2007, Bajo et al., 2019, Bajo et al., 2023; Roland et al., 2009; Ferrarin et al., 2013; Ferrarin et al., 2019; ; Ferrarin et al., 2023; Park et al., 2022; Arpaia et al., 2023; Cucco et al., 2023; 2024; Lagomarsino-Oneto et al., 2024).

The model solves the shallow water equations derived from the Navier-Stokes equations with the hydrostatic and Boussinesq approximations (Ferrarin and Umgiesser, 2005; Federico et al., 2017; Bajo et al., 2019).The shallow water equations are solved using a finite element numerical method and semi-implicit time stepping (Umgiesser et al., 2004). The model allows for different configurations of the governing equations (e.g., baroclinic formulation, three-dimensional) and various terms in the equations can be turned on/off such as the non-linear advection terms, baroclinic terms etc. (Ferrarin and Umgiesser, 2005; Ferrarin et al., 2013; Cucco et al., 2016; Cucco et al., 2023, 2024; Bajo et al., 2019; Bajo et al., 2023). The continuity and momentum equations in the conservative form are as follows:

$$\frac{\partial \zeta}{\partial t} + \frac{\partial (HU)}{\partial x} + \frac{\partial (HV)}{\partial y} = 0 \tag{1}$$

$$\frac{\partial (HU)}{\partial t} + \frac{\partial (HUU)}{\partial x} + \frac{\partial (HUV)}{\partial y} - fHV + gH\frac{\partial}{\partial x}\left(\zeta + \frac{p_a}{\rho_0 g}\right)$$

$$-\frac{\partial}{\partial x}\left(A_H H\frac{\partial U}{\partial x}\right) - \frac{\partial}{\partial y}\left(A_H H\frac{\partial U}{\partial y}\right) + UC_b\sqrt{U^2+V^2} - \frac{\tau_x^w}{\rho_0} = 0 \tag{2}$$

$$\frac{\partial (HV)}{\partial t} + \frac{\partial (HUV)}{\partial x} + \frac{\partial (HVV)}{\partial y} + fHU + gH\frac{\partial}{\partial y}\left(\zeta + \frac{p_a}{\rho_0 g}\right)$$

$$-\frac{\partial}{\partial x}\left(A_H H\frac{\partial V}{\partial x}\right) - \frac{\partial}{\partial y}\left(A_H H\frac{\partial V}{\partial y}\right) + VC_b\sqrt{U^2+V^2} - \frac{\tau_y^w}{\rho_0} = 0 \tag{3}$$

Here ζ is the water level, U and V are the depth averaged velocities in the x and y directions, g the gravitational acceleration, $H = h + \zeta$ the total water depth, h the undisturbed water depth, $t$the time, p_a the atmospheric pressure, ρ_0 is the standard water density, and C_b the friction coefficient, f is the Coriolis parameter, $A_H$the horizontal turbulent viscosity coefficient, computed by the Smagorinsky's formulation (Smagorinsky, 1963; Blumberg and Mellor, 1987) as suggested by Ferrarin et al. (2013) for similar applications. τ_x^w and τ_y^w are the wind stress components responsible for the vertical transfer of horizontal momentum at the surface of the fluid computed as:

$$\tau_x^w = \rho_{air} C_d W_x \sqrt{{W_x}^2 + {W_y}^2} \tag{4}$$

$$\tau_y^w = \rho_{air} C_d W_y \sqrt{{W_x}^2 + {W_y}^2} \tag{5}$$

where ρ_{air} is the density of air, C_d is the dimensionless wind drag coefficient, and W_x, W_y are the x, y components of the total wind velocity at a height of 10 m above sea level.

The differential equations are discretized using a semi-implicit discretization technique for stability reasons and a remarkable speed of execution (Umgiesser et al., 2004; Cucco et al., 2016; Bajo et al., 2019; Bajo et al., 2023). Specifically, in the two momentum equations (Eq. (2) and Eq. (3)), the Coriolis and the pressure gradient terms are treated semi-implicitly, the bottom friction is fully implicit, and the remaining terms are solved explicitly, while the divergence term in the continuity equation (Eq. (1)) is solved semi-implicitly. The terms explicitly treated in the momentum equation (e.g. advection, diffusion terms) are required to comply with stability constraints (Umgiesser et al., 2004). An in-depth treatment of the stability criteria can be found in Umgiesser et al. (2004). To this end, in our simulations a variable time-stepping procedure was employed, constrained to maintain the Courant-Friedrichs-Lewy (CFL) number below unity, sufficient to guarantee numerical stability.

Since the semi-implicit scheme is not mass conserving when using a normal finite element formulation for the spatial discretization, horizontal spatial integration is made using a staggered finite element approach based on a mesh composed of triangular elements (Umgiesser et al., 2004). Specifically, the spatial discretization follows a weak Galerkin formulation, with water levels and transports multiplied by their test function and integrated over each triangular element. Water levels are computed at the mesh vertices, while transports are computed at the centres of the elements, resembling the Arakawa-B grid configuration commonly used in finite difference schemes. The model uses basis functions of different orders: standard linear functions for water levels and stepwise constant functions for transports. A comprehensive description of SHYFEM's numerical scheme is provided in Umgiesser et al. (2004).

In this study, SHYFEM is set up to simulate the barotropic response to local forcing (combined wind and atmospheric pressure) and remote forcing (sea surface height and tidal forcing), thus excluding any sea level variability due to baroclinic processes such as temperature and salinity fluxes and freshwater discharge from rivers. At the closed boundaries of the model domain, the normal velocity is set to zero and the tangential velocity is a free parameter corresponding to a full slip condition. At the open boundaries the water levels can be prescribed in accordance with the Dirichlet boundary conditions and water transport is computed by the model in accordance with a radiative condition (Bajo et al., 2007).

2.3. Numerical experiments

2.3.1. Modelling strategy

Two computational domains have been considered; the first one spanning the entire North Atlantic Basin called the Basin Scale Model (BSM, panels A, B in Fig. 2) and a second domain confined to Donegal Bay called the Limited Area Model (LAM, panels C, D in Fig. 2). The primary focus of the storm surge modelling is the BSM, which covers the entire North Atlantic Basin and is exclusively driven by atmospheric forcing. This setup is specifically designed to accurately simulate the development and propagation of storm surges as storm systems traverse the North Atlantic, effectively capturing wind fetch effects critical for realistic surge representation within Donegal Bay (Kim et al., 2021). This modelling approach aligns with established methodologies where the numerical domain is exclusively forced with atmospheric data to simulate storm surges over large oceanic basins as already mentioned in the Introduction section.

In contrast, the LAM is utilized primarily as a comparative tool to assess the performance of the BSM through a predefined comparison run using default model parameters setting. As the BSM does not include tidal forcing, the LAM is used to quantify the errors in the BSM's residual

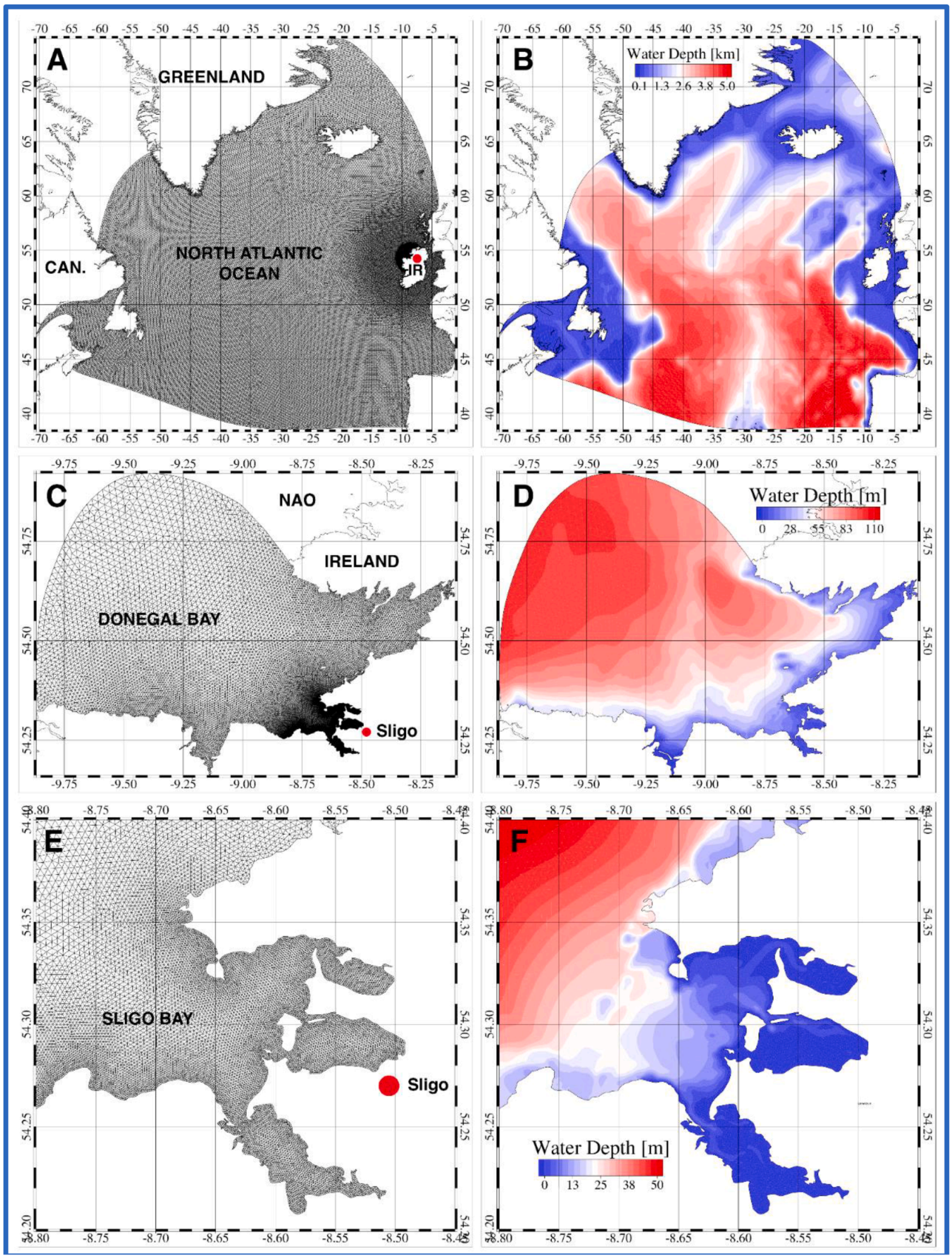

Fig. 2. Numerical Domain and the unstructured meshes for A) BSM, C) LAM, E) Sligo Bay and the corresponding depths of the respective basins (B, D, and F).

water level predictions that result from the omission of tidal contributions.

The comparison between the BSM and LAM is conducted on an ad hoc basis, without separate calibration of the LAM, to ensure that the BSM's outputs do not significantly deviate from expected behaviour. It should be noted that, due to the different extents of the two domains, optimal calibration parameters for C_d and C_b may vary. Despite this potential limitation, the approach remains valid, as previous studies comparing storm surge and wave simulations across different domain sizes did not adjust model calibration based on domain extent (Blain et al., 1994; Chen, 2022).

2.3.2. Numerical model setup

The computational meshes for both the BSM and LAM were generated using the GMSH package (Geuzaine and Remacle, 2009), with shorelines extracted from the Global Self-Consistent Hierarchical High-resolution Geography (GSHHG) dataset (Wessel and Smith, 1996). Bathymetric data were primarily sourced from the GEBCO dataset (GEBCO, 2022), a global terrain model for ocean and land with a spatial resolution of 15′ (approximately 450 m). To enhance accuracy within Donegal Bay, high-resolution bathymetric data (approximately 20–50 m) from the INFOMAR surveys (INFOMAR, 2024) were also incorporated. The combined bathymetric information was interpolated onto the computational mesh to produce the finite element grid used for model simulations.

Fig. 2 presents the computational meshes for the BSM and LAM along with the corresponding bathymetric details for the full model domains, which differ between the two configurations (panels A-D) and a zoomed-in view of Sligo Bay, located within Donegal Bay, where the meshes are almost identical (panels E-F).

The LAM consists of 40308 triangular elements and 21219 nodes. The resolution varies from 100–500 m in the region of interest and up to 2 km offshore. The BSM consists of 180158 elements and 92708 nodes. The resolution varies from 100–500 m in the region of interest up to 20 km offshore.

The main drivers of the storm surge in the LAM can be categorized into remote and local forcing (Park et al., 2022). Local forcing refers to the atmospheric field imposed as a surface boundary conditions, while remote forcing originates from the signals entering through the open boundaries, where the LAM is driven by hourly SSH data from CMEMS (Copernicus Marine Service, 2020) at a spatial resolution of 6–9 km.

The SSH signal includes 11 tidal constituents (M2, S2, N2, K1, O1, Q1, M4, K2, P1, Mf, Mm). The atmospheric boundary condition consists of six-hourly 10 m wind and mean sea level pressure fields provided by the Analysis dataset of the European Centre for Medium-range Weather Forecasts (ECMWF) at a spatial resolution of 0.25°, which combines the latest weather observations with a recent forecast to obtain the best possible estimate of the current state of the Earth system (Roberts et al., 2018; Bloemendaal et al., 2019; Dullaart et al., 2020). Residual water levels are obtained by applying harmonic analysis to the total water level output of the LAM.

The BSM employs closed boundaries (no normal flow) all along the mesh perimeter, where water levels are computed by SHYFEM with the normal velocity set to zero and the tangential velocity being a free parameter corresponding to a full slip condition. The same zero normal flow/full slip conditions are also applied where the mesh meets the open ocean, e.g., southern Atlantic perimeter, Labrador Sea, and Arctic Sea. This choice is justified as the potential influence of such artificial boundaries is minimised by using the large basin scale domain with such boundaries being located sufficiently far offshore from the study site to not influence the surges induced by the atmospheric forcings in the study area (Jensen, 1998). The BSM is exclusively forced with the same surface boundary conditions consisting of atmospheric fields from the ECMWF dataset for the simulation of the residual water levels.

Although significant improvements in storm surge prediction have been demonstrated through the coupling of tidal dynamics with wind and pressure driven water level dynamics (Fernández-Montblanc et al., 2019), this approach was not applied to the BSM due to the extensive size of its computational domain. Notably, improvements resulting from coupling tidal and atmospheric forcing are most pronounced in regions where tide-surge interactions are significant (Brown et al., 2010b; Haigh et al., 2010).

A preliminary evaluation of the extent of tide-surge interaction in this specific study site was performed using tide gauge observations and applying the method proposed by Dixon and Tawn (1994) which has been widely adopted in other studies (Haigh et al., 2010; Costa et al., 2023; see Appendix A1).

Simulations for both BSM and LAM were performed for the years 2007–2021 for model validation and comparison between the BSM and LAM at all the four tide gauges. Specifically, the year 2020 was used for calibrating the models' parameters which is detailed in the following Section 2.4.

The model outputs from both the BSM and LAM are available at an hourly frequency. Accordingly, observational data were averaged to the same temporal resolution to enable consistent comparison with the modelled results. The observations from the tide gauges and the Limited Area Model (LAM) outputs represent total water levels, comprising of tidal signals, atmospheric (meteorological) contributions, and other low-frequency and low amplitude sea level variations (Bajo et al., 2019). In contrast, the Basin Scale Model (BSM) outputs represent only the atmospheric component and are therefore more appropriately referred to as residual water levels or sea level residuals (Ratsimandresey et al., 2008; Bajo et al., 2019; Pinheiro et al., 2020; Feng et al., 2021). Here the term "residual water level" will be used throughout for consistency.

To enable a consistent comparison between BSM outputs, observations, and LAM simulations, the tidal component is removed from the total water level time series, for both the observed and modelled outputs of the LAM, yielding residual water levels. These residuals from the tide gauge records and the LAM contain not only the contributions from atmospheric forcings but also other low-frequency and low-amplitude sea level components, which are negligible compared to the meteorological contribution during intense storm events (Bajo et al., 2019).

Pugh and Woodworth (2014) states that the term "surge" or "storm surge" is used for a particular event during which a very large non-tidal component (residual water level) is generated. In the context of this study, the term "surge" or "storm surge" refers specifically to the residual water level exceeding a predefined threshold, indicating significant storm-induced elevation. This threshold corresponds to values above the 99th percentile of the observed residual water levels over the analysis period, as computed in the following Section 2.4.

2.4. Model calibration and validation

2.4.1. Model error quantification and extreme value analysis

Model performance against observations is quantified with four statistics: root mean square error (RMSE), average bias (BIAS), Pearsons' correlation (R), and the model skill (k) (Warner et al., 2005). The corresponding formulae are described in Appendix (Table A1).

To evaluate model's ability to simulate observed surge extremes a Q-Q plot (Wilk and Gnanadesikan, 1968) is used for comparison, and the Generalized Pareto Distribution (GPD) is employed to calculate observed and modelled return level values. Q-Q plots help assess whether observed and modelled residual water levels share the same distribution. If the points align along the identity line $y = x$, the distributions are similar. A straight line with a different slope or intercept indicates the same distribution shape but differing scale or location, suggesting that the model can be calibrated. However, deviations from a straight line imply different distribution shapes, making calibration difficult and reducing the model's reliability for extreme value analysis and future projections (Calafat et al., 2014).

The GPD (Coles, 2001) models the tail of the distribution of the residual water levels above a given threshold (surges). The cumulative

distribution function is:

$$F(x;\xi,\sigma,u) = 1 - \left(1 + \frac{\xi(x-u)}{\sigma}\right)^{\frac{-1}{\xi}} \quad (9)$$

where x is the surge observation exceeding the threshold u, σ ($\sigma>0$) is the scale parameter, and ξ is the shape parameter. The scale and shape parameters are estimated by the maximum likelihood technique. Before the parameter estimation, a declustering window of 24 h is applied to ensure independence of the extreme surge events following O'Brien et al. (2018) and Cid et al. (2016), since storm surges in Ireland are usually seen to last up to 24 h. 24 h is also the time window automatically detected for declustering by the R package, ExtRemes 2.0 (Gilleland and Katz, 2016) used for extreme value analysis in the present work. The N year return level (RL_N) can be estimated by:

$$RL_N = F^{-1}\left(1 - \frac{1}{\lambda N}; \xi, \sigma, u\right) \quad (10)$$

where λ is the mean number of exceedances of the threshold per year.

Calafat et al. (2014) calculated the return levels for return periods of 10 and 50 years considering approximately 25 years of observed data, which is also reasonable for our case given that tide gauge records only begin around 2007 up to present implying under 20 years of records, so calculation of longer return levels may not be reliable even though longer return levels for up to 500 years have been calculated from around only 8 years of tide gauge data (Tsimplis and Blackman, 1997). Return levels for 5 (RL_5), 10 (RL_{10}), 25 (RL_{25}), and 50 (RL_{50}) year return period values have been hence calculated. In Ireland 0.5 m of surge exceedances are candidate storm surge events responsible for coastal flooding (Olbert and Hartnett, 2010) and from an analysis of the observations from the tide gauges within Donegal Bay, such a threshold is met by the residual water levels higher than the 99th percentile value (Marcos et al., 2009; Haigh et al., 2010; Calafat et al., 2014). Thus, we used 0.5 m for the GPD threshold, similar to Lin et al. (2010), and the performance of the GPD model for such a threshold was evaluated through diagnostic plots provided by the R package, ExtRemes 2.0 (Gilleland and Katz, 2016).

Furthermore, the mean differences of the observed and modelled residual water levels are expressed as a function of the observed residual water levels categorised into 0.1 m bins. This implies that a bin centred at 0.55 m will reflect the mean and standard deviations of the differences (observed-modelled) in the range [0.50 m, 0.60 m]. This helps in quantifying any over/underestimation of the modelled residual water levels with respect to the observations.

2.4.2. Trial and error sensitivity analysis and calibration

A trial-and-error calibration approach has been adopted for the BSM to assess improvements in the accuracy of the modelled residual water levels.

The model parameters varied during the calibration process were the wind drag (C_d) and bottom friction coefficients (C_b). Initial model evaluation was performed for the model setup of the BSM and LAM with both coefficients set to the default value of 0.0025, a commonly adopted value in the storm surge modelling literature (Olbert and Hartnett, 2010; Calafat et al., 2014; Sannino et al., 2022) This configuration is hereafter referred to as the "default calibration run".

First-order model validation and estimation of tide-surge interaction were performed using the default setup by comparing BSM and LAM results over the full observation period (from 2007 to 2021), based on data from four tide gauges located at Sligo, Killybegs, Ballyglass, and Aranmore.

Subsequently, a series of calibration runs were conducted exclusively for the BSM to improve its ability to simulate residual water levels including extreme events. These runs involved varying the C_d and C_b, with model results compared against observations. The calibration was performed with respect to the year 2020 and focused specifically on the Sligo tide gauge, due to its proximity to the vulnerable Donegal Bay coastline, which is undergoing active coastal erosion (Tiwari et al., 2025).

The year 2020 was selected since it presents the highest number of independent surge exceedance events, eight exceeding 0.5 m, including two above 1 m, making it a particularly suitable period for tuning the model to storm surge conditions in the region.

The calibration of the BSM was performed in two steps:

Initial Parameter Variation:

In the first step, a sensitivity analysis was conducted by varying one parameter while keeping the other fixed at its default value (0.0025). Specifically, the wind drag coefficient C_d was held constant while varying the bottom friction coefficient C_b, and vice versa. Both parameters were varied across a wide range from 0.000001 to 0.01, encompassing values commonly used in storm surge simulations (Lowe et al., 2001; Olbert and Hartnett, 2010; Muis et al., 2019).

Best Parameter Selection and Combination Runs:

Based on the results of step (i), the three best-performing values for C_d and C_b were identified. These were then paired in all possible combinations, resulting in nine additional BSM simulations. In total, this iterative calibration procedure produced 25 BSM simulation runs for the year 2020 (see Appendix Table A2).

For the LAM, such calibration was not undertaken, as it is not intended for future climate projection studies. A subset of the 2020 calibration runs that demonstrated high skill scores was validated over the full observation period, allowing for evaluation of the impact of C_d and C_b on model performance.

The results of the 25 BSM runs were visualized using a Taylor diagram (Taylor, 2001), which simultaneously displays the standard deviation, correlation coefficient, and centred root mean squared error (CRMSE) between modelled and observed data. This visualization provides a comprehensive assessment of the model's sensitivity to variations in the drag and friction parameters.

3. Results

3.1. Storm surge and their interaction with the tides from observations

In this section, the results from the preliminary analysis conducted using the method proposed by Dixon and Tawn (1994) to quantify the extent of tide-surge interaction, based on tide gauge observations is presented. The results from the χ^2 test at a 99th percentile threshold of the residual water levels (surges) shows no significant tide-surge interaction as seen from Fig. 3 and the values of the χ^2 test statistic from Table 1. The χ^2 test statistic is <9.5 even at higher thresholds (99.95 and 99.9 percentile) for all sites within the bay Table 1.

Fig. 3 shows the distribution of the residual water level (surge) exceedances above the 99th percentiles across all sites against the corresponding tidal level. For instance, for Sligo the number of events above the 99th percentile is 971, so in each tidal band the number of expected events would be 194, assuming that tide-surge interaction is negligible. Indeed, there is no drastic variation in the number of such exceedances for each tidal band, and the same pattern is mirrored across the other sites showing negligible tide-surge interaction resulting in low values of the χ^2 test statistic (Table 1).

The kernel density estimates (Dixon and Tawn, 1994) of the residual water levels at the four Donegal Bay tide gauge stations (Sligo, Killybegs, Ballyglass, and Aranmore) produce unimodal, zero-mean distributions once tidal components are removed. At Sligo and Killybegs, the distributions exhibit moderate positive skew, 0.714 and 0.657, respectively with maxima just above 1 m. Their interquartile ranges (0.195 m and 0.199 m) and standard deviations (0.155 m and 0.161 m) reflect a pronounced right tail and substantial overall variability. Ballyglass shows the tightest clustering around zero (skewness = 0.415; IQR = 0.191 m; SD = 0.148 m), indicating a more symmetrical residual water

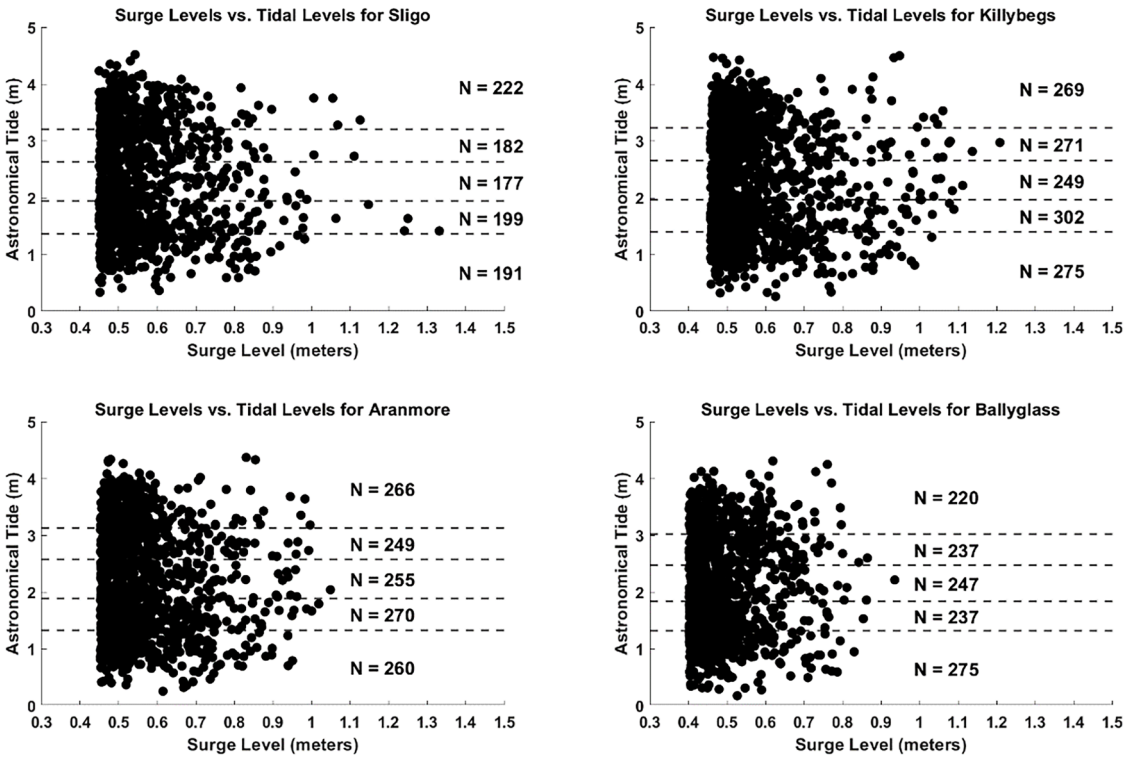

Fig. 3. Surge level for all residual water levels exceeding the 99th percentile plotted against the associated astronomical tidal level for Sligo, Killybegs, Ballyglass, and Aranmore.

Table 1
Tide-surge interaction χ^2 test statistic for surge events greater than the 99th, 99.95th and 99.9th percentiles of the residual water levels.

Site	χ^2 test statistic		
	99th percentile	99.95th percentile	99.99th percentile
Sligo	6.441	5.796	9
Killybegs	5.274	1.412	7.429
Aranmore	1.085	2	3.539
Ballyglass	6.747	2.689	2.167

level signal. In contrast, Aranmore combines the greatest dispersion (IQR = 0.209 m; SD = 0.165 m) with positive skewness (0.608), evidencing both a wide central spread and occasional large positive residuals. Overall, these findings demonstrate that tide-surge interaction is statistically non-significant at all sites in Donegal Bay, and that residual water level distributions are unimodal, zero-mean, and positively skewed with site-specific variability.

3.2. Storm surge hindcasts from basin scale model and limited area model

Firstly, the domain of the LAM purely forced by atmospheric data extended just to the continental shelf is clearly insufficient to capture the surge formation as most depression systems over the NE Atlantic are generated far west off the continental shelf (Olbert and Hartnett, 2010). This is clearly seen from Fig. 4 where the residual water level response for the atmospheric (ATM) only forcing of the LAM for 2020 is underestimated. The inadequacy of the residual water level response due to atmospheric only forcing required imposing at the open boundary of the LAM with SSH data from another deep-water ocean model to reproduce the historical surges near shore within the bay.

The residual water levels from the numerical simulations for both the BSM and the LAM, using the default calibration run, were compared against the observations from the tide gauges. A qualitative comparison of the observed and modelled residual water levels at Sligo, Killybegs, Ballyglass and Aranmore over the period 2007 to 2021, shows that both the LAM and BSM can capture the variability of the residual water levels reasonably well (see Appendix Figure A2; only modelled residual water levels for the corresponding time stamps of the observations are shown, thus also highlighting any gaps in the observation records).

Quantitative comparison is summarized in Table 2. The values of the correlation for the residual water level time series for the whole observation period shows reasonably good correlation for both the models, with LAM showing higher correlation than the BSM across all the four tide gauge stations. LAM exhibited minimal bias across all stations, with values close to zero, indicating well-calibrated predictions. Specifically, the LAM model produces a slight underprediction of residual water levels at Sligo (−0.003 m) and Ballyglass (−0.001 m), and a small overprediction at Killybegs (0.005 m) and Aranmore (0.006 m) and in contrast the BSM consistently exhibits a positive bias at all stations, pointing to a systematic overprediction of the residual water levels. The bias values ranged from 0.003 m at Ballyglass to 0.038 m at Aranmore. At Sligo (0.026 m) and Killybegs (0.033 m), the BSM model showed a moderate overestimation of the residual water levels.

From Table 2 the LAM shows overall higher correlation, lower RMSE's and lower bias values for the residual water levels as compared to the BSM. This is because when no intense atmospheric forcing is acting, the major contributor to the residual water level is due to the impact of baroclinic pressure gradients imposing gentle free-surface slopes (Pringle et al., 2019). This kind of signal, detectable in the observations is also accounted in the LAM which used OBC derived from a baroclinic deep water ocean model. The BSM, on the other hand, forced only by atmospheric fields, cannot reproduce these low-frequency residual fluctuations and consequently its accuracy is slightly reduced in the overall time series (Pringle et al., 2019). Thus, the difference in the RMSE values between the residual water levels of the LAM and the BSM which is within ~3 cm (Table 2) is not entirely due to the non-inclusion of tides, as the tide-surge interaction in the bay from the preliminary analysis of the tide gauge observations has been found to be negligible

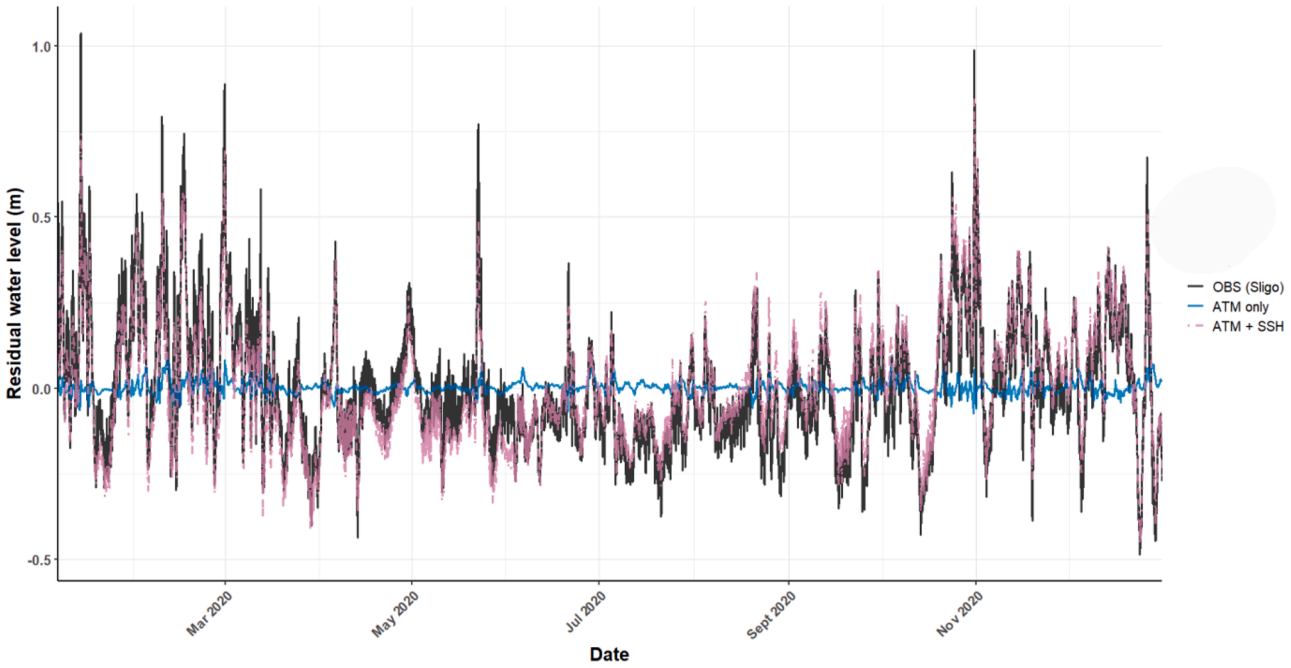

Fig. 4. Residual water level response at the Sligo tide gauge from the LAM outputs forced with atmospheric forcing (ATM) only and combined atmospheric forcing at the surface and Sea Surface Height at open boundary (ATM + SSH).

Table 2
Error metrics for the comparison of the residual and total water level time series between the LAM and BSM (total water levels constructed for BSM by linearly adding the residual water levels to the reconstructed tides from the tide gauge stations) at the four tide gauge stations for the period 2007–2021.

Metric	Model	Sligo		Killybegs		Ballyglass		Aranmore	
		Residual water levels	Total water levels	Residual water levels	Total water levels	Residual water levels	Total water levels	Residual water levels	Total water levels
LAM									
P. corr		0.788	0.971	0.813	0.966	0.808	0.969	0.824	0.974
RMSE (m)		0.101	0.237	0.096	0.256	0.091	0.228	0.096	0.228
Bias(m)		−0.003	0.002	0.005	−0.011	−0.001	0.001	0.006	0.001
Skill score		0.885	0.985	0.900	0.982	0.896	0.984	0.906	0.986
BSM									
P. corr		0.763	0.992	0.781	0.991	0.768	0.993	0.803	0.993
RMSE (m)		0.121	0.128	0.122	0.141	0.107	0.134	0.123	0.141
Bias(m)		0.026	0.038	0.033	0.054	0.003	0.042	0.038	0.081
Skill score		0.860	0.996	0.866	0.994	0.869	0.995	0.875	0.994

(Fig. 3 and Table 1). As already explained in Section 2.3.1, the default calibration may not necessarily be a near optimal calibration for the BSM, implying that the error metrics of the BSM could improve with calibration. While the default calibration for the LAM may not be optimal, substantial improvement in performance from additional calibration are not foreseen. This is because the open boundary is located near the coastline and already incorporates most of the relevant residual water level information. Although further calibration might yield minor improvements, significant enhancement in model performance is unlikely under these boundary conditions. This can be understood from an analysis of the SSH data from CMEMS that was used as an OBC for the LAM. SSH data from the closest available grid points for the Sligo and Killybegs tide gauges were extracted directly from the CMEMS dataset. The residual water levels derived following a harmonic analysis was compared against the observations for quantifying the error metrics. These error metrics are compared against the error metrics obtained for the modelled outputs of the LAM just for the year 2020 as shown in Table 3 (see Appendix Figure A3).

As seen the residual water level outputs from the CMEMS dataset compares quite well with the observations, though naturally the ones from the modelled data shows better performance as it downscales the SSH data from the deep-water ocean model (which is a finite difference baroclinic ocean model) enabling the LAM to better resolve the complex

Table 3
Error metrics of the residual water levels from CMEMS against observations and the modelled LAM output.

Metric	Sligo		Killybegs	
	CMEMS vs Observed	Modelled LAM vs Observed	CMEMS vs Observed	Modelled LAM vs Observed
P. corr	0.877	0.905	0.89	0.965
RMSE (m)	0.088	0.078	0.086	0.049
Bias (m)	0.001	−0.0002	0.001	0.0002

Donegal Bay coastline. Thus, the short domain and the pronounced influence of the OBCs in the LAM limit the impact of further adjustments to C_d and C_b. As a result, drastic changes in model performance due to variation of these coefficients are unlikely, since the primary variability is already captured by the residual water level information in the OBC.

Given the negligible tide-surge interaction as demonstrated through both the analysis of tidal data (Section 3.1) and comparisons of the residual water levels between LAM and BSM (Table 2), tides can be linearly added to the residual water levels in the BSM to compute total water levels (Marcos et al., 2012), enabling direct comparison with the total water levels produced by the LAM. Total water levels directly obtained from LAM and ones by adding reconstructed tides and residual water levels from BSM were demeaned to mean sea level zero, enabling direct comparison of total water levels relative to zero mean sea level as shown in Table 2. The total water levels generally show higher correlation for both the LAM and BSM compared to the residual water levels because the hydrodynamics in the bay is tidally dominated. Additionally, the RMSE values are lower for the BSM than for the LAM, mainly because the tides added to the BSM are reconstructed from tide gauges (observations) with around 60 tidal constituents, making them naturally more accurate.

From Table 2, both the LAM and BSM are seen to capture the trends in the residual water levels reasonably well, but this does not necessarily translate for the extremes (Calafat et al., 2014). Mean difference plots from Fig. 5, for both the LAM and BSM models show increasing mean differences as the magnitude of the residual water level increases, with the magnitude of underestimation (positive differences) growing in the higher residual water level bins (above approximately 0.5 m). This suggests that both models struggle to accurately capture the magnitude of larger surge events. The results of these mean difference plots are similar to those reported by Marcos et al. (2012), thus highlighting a significant challenge in storm surge modelling, particularly for extreme events. The underestimation observed at Sligo and Killybegs for the highest residual water level (surge) bins is consistent with the well documented limitations of traditional surge models to underestimate the extremes (Debernard et al., 2002; Marcos et al., 2009; Muis et al., 2016).

At the Sligo gauge the underestimation is most pronounced, with the mean difference between observed and modelled residual water levels increasing progressively with the observed magnitude of the residual water levels. In the highest bins (approximately 1.2 m), the BSM underestimates surge heights by >0.5 m This substantial discrepancy suggests that the BSM struggles to accurately simulate the most extreme surges at this location. A similar pattern of underestimation is observed at the Killybegs station, where the BSM underpredicts surge heights by nearly 0.6 m in the highest bins. In contrast, the Ballyglass and Aranmore stations demonstrate a stable mean difference, remaining below 0.3 m Overall, surge magnitudes are frequently underestimated by both the LAM and BSM models. The degree of underestimation increases in larger residual water level bins, particularly over ~ 0.6 m. The BSM model exhibits more pronounced underestimations at higher residual water levels, particularly for stations such as Sligo and Killybegs, where deviations grow dramatically for surges greater than 1.0 m. In contrast, the LAM performs more consistently across all stations, with fewer major underestimations in the upper residual water level bins than the BSM. Aranmore has the smallest difference between observed and modelled values for both models, indicating improved overall performance. Ballyglass behaves similarly, with moderate underestimations in both models, albeit LAM performs significantly better in terms of capturing larger surges.

Since the main focus is to examine the ability of the BSM for projection of storm surges under changing climate scenarios, comparison of climatological statistical quantities like return levels derived from extreme value analysis of the modelled outputs with the observed data is of foremost importance and after visual examination with Q-Q plots reveals the feasibility of such extreme value analysis. From Fig. 6, the Q-Q plots for the BSM across different locations show that the majority of the points are scattered tightly around the identity line, suggesting that the BSM reproduces the distribution of observed residual water levels. There are some slight deviations from the line at the highest quantiles, particularly at Sligo and Killybegs, which indicate a small underestimation of the most extreme events. However, the overall alignment with the identity line suggests that the BSM is robust for modelling surge extremes, as it captures both moderate and extreme values of the residual water levels accurately. The deviations are minor, indicating that with some small adjustments, the BSM model could perform even better at capturing the largest surges. In contrast, the Q-Q plots for the LAM display more pronounced divergence at the upper quantiles, especially in Sligo and Killybegs. However, the LAM exhibits near perfect alignment with the identity line for Ballyglass followed by Aranmore indicating superior calibration performance at these locations. This is further supported by the LAM's mean difference plots shown in Fig. 5.

Table 4 presents the return levels calculated for return periods of 5, 10, 25 and 50 years for both the LAM and BSM models at the tide gauge stations. As mentioned previously for the calculation of the return levels, a threshold of 0.5 m was imposed on the residual water levels with a declustering window of 24 h and the GPD fit was evaluated through diagnostic plots like Q-Q plots showing good agreement (not shown here) between the data (empirical quantiles) and the GPD model (model quantiles) for the observations and modelled outputs from the LAM and BSM.

The LAM model consistently underestimates return levels, particularly in Sligo and Killybegs, with the gap widening for higher return periods (e.g., Sligo RL_{50}: 1.249 m observed vs. 0.916 m modelled). For Ballyglass the return levels are near perfect with the observations almost as expected from the Q-Q plots, thus showing the best alignment followed by Aranmore with moderate underestimation which increases with increasing return periods. In contrast, the BSM generally performs better across all the tide gauge stations, especially for longer return periods, with only Sligo showing a slight overestimation of around 7 cm at RL_{50} (1.249 m observed vs. 1.322 m modelled). For Killybegs (similar to Sligo) for RL_5 and RL_{10} while the model underestimates by greater than 10 cm, this gap is dramatically reduced for RL_{25} and RL_{50}, thus displaying more consistent results. At Ballyglass like the LAM, the return levels for the BSM are nearly perfect compared to the observations, followed by Aranmore. Overall, the BSM model is much more accurate in reproducing the observed return levels across all the sites, particularly at Sligo and Killybegs as compared to LAM.

From the above results, the BSM performs well in terms of capturing the long term statistical properties of the extremes for the simulation period and demonstrates that it can accurately reproduce the climatological statistics of storm surges and can thus be used for storm surge projections under changing climate scenarios. This however does not necessarily imply that the model simulates the individual extreme events accurately at specific time stamps (Calafat et al., 2014; Campos-Caba et al., 2024). There may be phase errors, defined as discrepancies between the timing or phase of simulated storm surge events and their actual occurrence in observational data (Campos-Caba et al., 2024). Such errors are particularly critical for operational storm surge forecasting, where accurate timing is essential (Calafat et al., 2014; Vousdoukas et al., 2016). However, this aspect lies outside the scope of the present study. Therefore, phase errors are not investigated here and the ability of the BSM to have accurately captured the overall distribution and severity of storm surge extremes is sufficient to meet the objectives of the present research.

Model calibration at Sligo was considered worthwhile, especially given the significant underestimation and variability in the simulation of the extreme surge events observed in the current BSM setup, while at the same time being cognizant that changes made to improve performance at Sligo might still impact the model's performance at other stations.

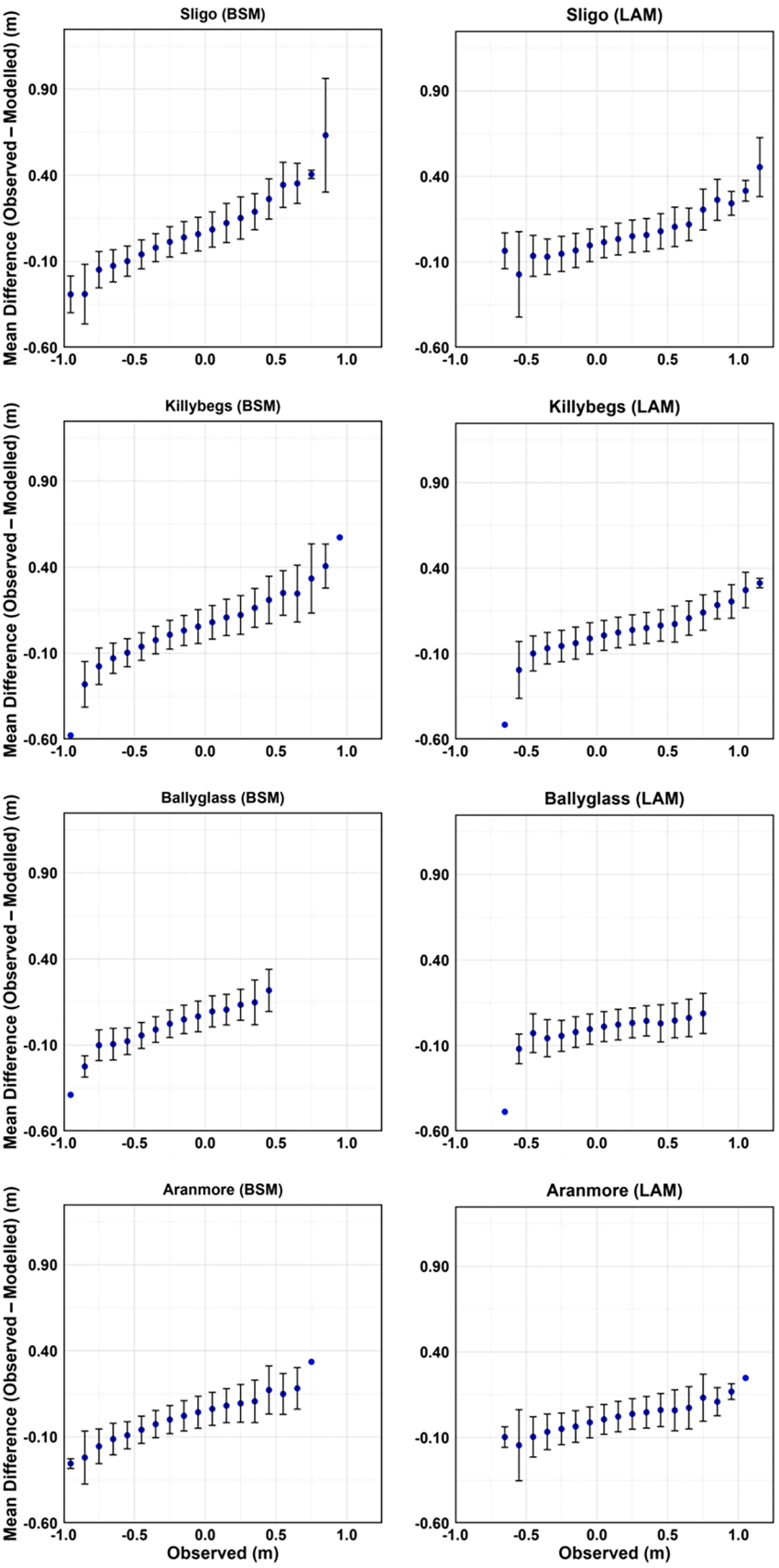

Fig. 5. Mean difference plots for the BSM and LAM for the default calibration. The error bars represent the standard deviation of the means and are only shown when there are at least three values.

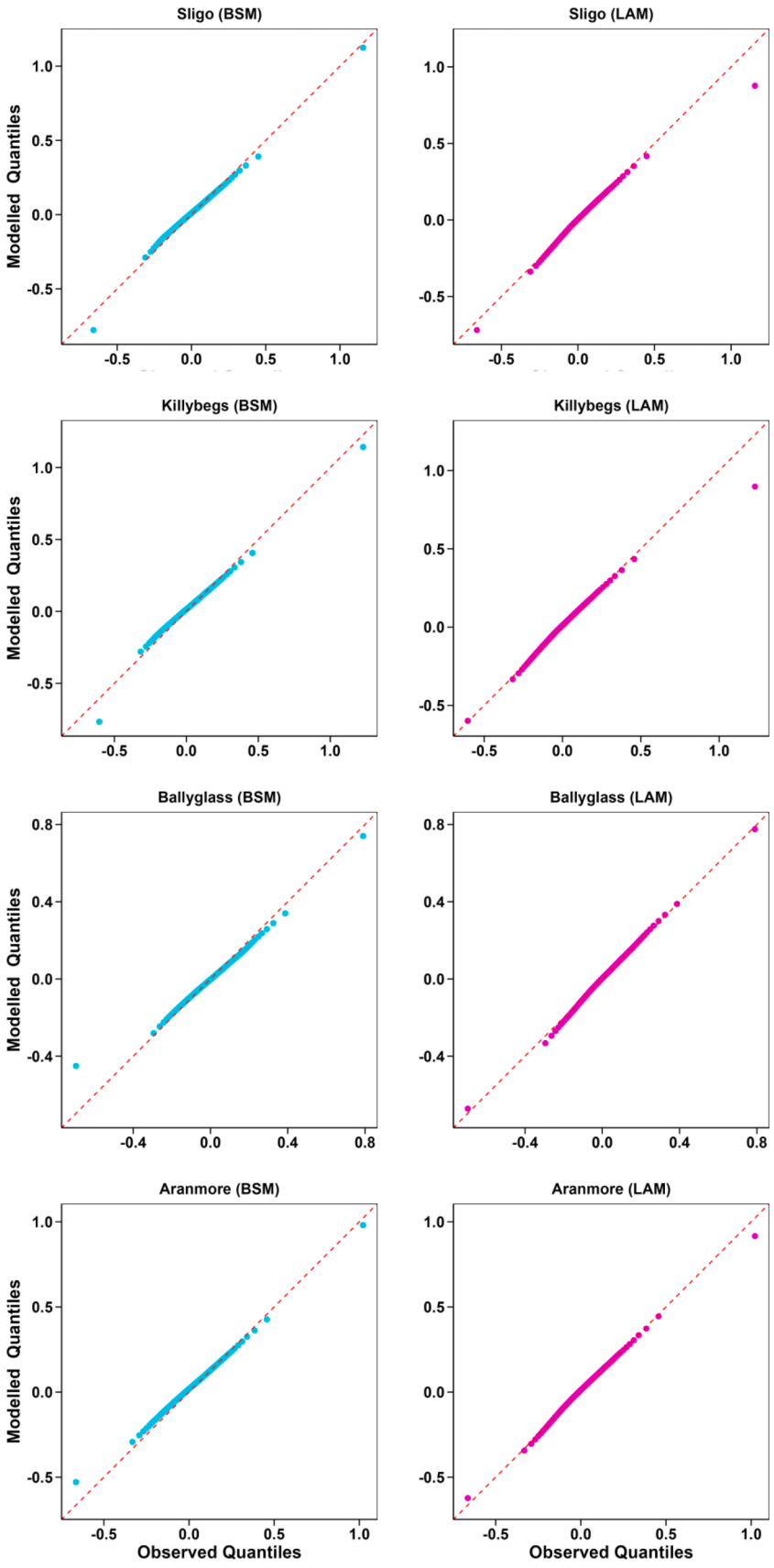

Fig. 6. Q-Q plots of the Observed vs Modelled quantiles of the residual water levels for the LAM and BSM.

Table 4
Return levels (m) calculated for return periods of 5, 10, 25, and 50 years for a declustering window of 24 h for the LAM and BSM at Sligo, Killybegs, Ballyglass and Aranmore tide gauge stations.

Model	Station	RL_5		RL_{10}		RL_{25}		RL_{50}	
		OBS	MODEL	OBS	MODEL	OBS	MODEL	OBS	MODEL
LAM	**Sligo**	1.044	0.793	1.114	0.836	1.195	0.885	1.249	0.916
	Killybegs	1.068	0.837	1.159	0.874	1.273	0.913	1.353	0.935
	Ballyglass	0.742	0.735	0.764	0.756	0.783	0.773	0.792	0.782
	Aranmore	0.937	0.853	0.997	0.896	1.067	0.943	1.114	0.971
BSM	**Sligo**	1.044	0.889	1.114	1.003	1.195	1.175	1.249	1.322
	Killybegs	1.068	0.937	1.159	1.05	1.273	1.213	1.353	1.347
	Ballyglass	0.742	0.678	0.764	0.706	0.783	0.73	0.792	0.741
	Aranmore	0.937	0.867	0.997	0.93	1.067	1.005	1.114	1.056

3.3. Assessing BSM's accuracy to varying model parameters

The calibration of the BSM within Donegal Bay was therefore undertaken with a focus to examine any improvement in the accuracy of simulated storm surge extremes, particularly at the Sligo tide gauge. The calibration process involved varying the wind drag (C_d) and bottom friction (C_b) coefficients, targeting the residual water level time series, and the surge levels at 0.5 m and 0.75 m for the year 2020. The iterative trial and error method resulted in a total of 25 calibration runs for the BSM (see Appendix Table A2). The response of the BSM to the different parameterization can be seen through the Taylor diagram from Fig. 7. The table with error metrics for the whole set of simulations is presented in the Appendix Table A2. From the Taylor diagram (in Fig. 7), the legends have been omitted to avoid visual clutter and to focus on illustrating the sensitivity of the BSM to variations in C_d and C_b. The high sensitivity of the BSM to the tuning parameters is prominent, this is expected given that it is driven purely with atmospheric forcings. Furthermore, it is also seen that some simulations are clustered closely together with the implication that certain combinations of the C_d and C_b could lead to comparable outputs with the observed data.

A set of calibration runs with high skill scores were considered on an ad hoc basis for evaluating changes in the accuracy of the modelled outputs for the entire observed period of the Sligo tide gauge. The simulations considered were sim 11, sim 12, sim 13 and sim 14 (see Appendix Table A2) corresponding to values of 0.004 & 0.0075, 0.005 & 0.0025, 0.005 & 0.005, and 0.005 & 0.0075 for C_d and C_b, respectively. The error metrics of the modelled residual water levels for the BSM for these selected calibration runs for the entire observed period of the Sligo tige gauge are presented in Table 5. The default calibration run has been repeated again for a clear comparison of the differences in modelled

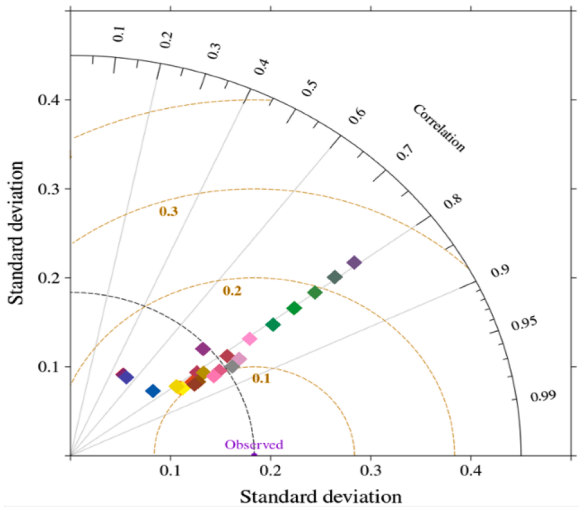

Fig. 7. Taylor diagram for the BSM versus observed residual water levels (2020). Dashed golden arcs show CRMSE contours.

Table 5
Error metrics of the residual water level time series of the BSM at the Sligo tide gauge station for the observed period by varying the C_d and C_b.

Calibration runs	P. corr	RMSE(m)	Bias(m)	Skill Score
0.0025 & 0.0025	0.763	0.121	0.026	0.860
0.004 & 0.0075	0.787	0.103	0.023	0.880
0.005 & 0.0025	0.725	0.141	0.020	0.830
0.005 & 0.005	0.764	0.121	0.026	0.861
0.005 & 0.0075	0.778	0.114	0.030	0.870

outputs by varying the C_d & C_b. Improvements in the error metrics are seen for runs 0.004 & 0.0075 and 0.005 & 0.0075 hence showing the influence of model calibration on the simulated residual water levels. These results are mirrored in the return level values from Table 6.

The results for the Q-Q plot and mean difference plots for all these calibration runs are presented in Appendix (Figure A4 and Figure A5).

From Table 6, on comparing the default calibration runs with the other calibration runs, where the underestimation is >10 cm for the RL_5 and RL_{10} values with the model's performance improving for RL_{20} and RL_{50} as explained previously. The calibration run 0.004 & 0.0075 shows the best performance with improved performance across all return levels. RL_5 and RL_{10} differences are minimal, at 0.025 m and 0.003 m, respectively. The model slightly overestimates RL_{25} by 0.039 m and RL_{50} by 0.079 m, but these deviations remain relatively small, indicating strong alignment with observed values at this calibration setting. For 0.005 & 0.0025, the model consistently overestimates across all return levels, with the largest differences seen at RL_{25} (0.143 m) and RL_{50} (0.148 m). The model overestimates RL_5 and RL_{10} by 0.139 m. This indicates that the model begins to overshoot return levels as the C_d increases without making changes to the C_b (by keeping it at its default value of 0.0025). As the value of the C_b increases, improvements are seen for 0.005 & 0.005, but the model still continues to overestimate all return levels, with RL_5 showing a difference of 0.089 m and RL_{10} at 0.099 m. The RL_{25} and RL_{50} differences are 0.118 m and 0.135 m, respectively. This run shows improved performance over the previous but still remains biased towards overestimation, particularly for higher return levels. Increasing the C_b further shows improvements, though 0.005 & 0.0075 still shows a similar overestimation pattern with RL_5 and RL_{10} differences of 0.060 m and 0.071 m, respectively. RL_{25} and RL_{50} show larger overestimations of 0.092 m and 0.112 m. Despite the persisting overestimation, this run shows better alignment than the 0.005 & 0.0025 and 0.005 & 0.005 runs, especially for lower return levels.

The results on the return levels are reflected in the Q-Q plots (see Appendix Figure A4), where the 0.004 & 0.0075 calibration shows a closer alignment with the identity line, indicating better model performance. In contrast, the 0.005 & 0.0025 calibration displays deviations from the identity line, with noticeable change in shape, suggesting a decline in performance thus mirrored in the return levels. As the distribution approaches the identity line, model performance improves. Additionally, the influence of calibration on the modelled residual water

Table 6
Return levels for a set of different calibration runs by varying the Cd & Cb for the BSM.

Calibration runs	RL_5		RL_{10}		RL_{25}		RL_{50}	
	OBS	MODEL	OBS	MODEL	OBS	MODEL	OBS	MODEL
0.0025& 0.0025	1.044	0.889	1.114	1.003	1.195	1.175	1.249	1.322
0.004& 0.0075		1.019		1.111		1.234		1.328
0.005& 0.0025		1.183		1.253		1.338		1.397
0.005 & 0.005		1.133		1.213		1.313		1.384
0.005& 0.0075		1.104		1.185		1.287		1.361

levels is evident in the mean difference plot especially for the calibration runs with C_d= 0.005 across the moderate residual water level bins where the mean difference hovers close to zero (see Appendix Figure A5). Thus, careful calibration tuning impacts model accuracy.

4. Discussion

The Basin Scale Model (BSM) configuration is specifically designed to be exhaustive in accurately capturing the development and passage of storm systems across the North Atlantic contributing to storm surges within Donegal Bay.

Few studies have assessed domain size effects on storm surge response. Limited area models (LAMs) remain commonly used for computational efficiency, despite limitations in surge accuracy (Blain et al., 1994; Morey et al., 2006; Kerr et al., 2013; Liao and Kaihatu, 2016). For example, Blain et al. (1994) found that models with smaller domains on the continental shelf significantly underestimate storm surge responses as is the case with the LAM (Fig. 4), while larger domains accurately capture surge effects. To mitigate the inadequacy in the surge response, LAMs require OBCs with suitable spatio-temporal resolution to resolve the storm surge signal which are available only at a monthly frequency from the climate models thus limiting the utilisation of LAMs for the projection of storm surges under future climate scenarios.

Since atmospheric fields at a higher temporal resolution are easily available from climate models, BSMs driven exclusively by the atmospheric fields are thus currently used within state of the art storm surge projection studies (Vousdoukas et al., 2016). Whether or not to include tides within the BSM modelling approach depends on the significance of tide-surge interaction within the study site.

There are limitations pertaining to the accurate simulation of tidal phases and amplitudes for such a large oceanic basin (Kirstensen et al., 2024) and thus the increased complexity and computational times from including the tidal components in the simulation may outweigh the potential gains in data quality (Vousdoukas et al., 2016) especially for such studies where the simulation of the statistical properties of storm surge extremes, i.e., the overall distribution and severity of extreme events is the main priority. The LAM approach was adopted in this study just to quantify the tide-surge interaction without the intention of using it for climate projection due to reasons already mentioned in the Introduction.

The RMSE for the BSM model is higher than that of the LAM model by 0.020 m at Sligo, 0.026 m at Killybegs, 0.016 m at Ballyglass, and 0.027 m at Aranmore for the hindcast residual water levels for the default calibration run. These differences are within ~3 cm which is in agreement with the results from Fernández-Montblanc et al. (2019), where they found improvements in the RMSE within 3 cm by coupling tides.

While such improvements are typically attributed to the inclusion of tide-surge interaction, the preliminary analysis of tide gauge records for Donegal Bay indicates that tide-surge interaction is statistically non-significant at this site.

Consequently, the observed ~3 cm difference can be also attributed to the BSM, which is forced exclusively by atmospheric fields, and therefore unable to capture the low-frequency and amplitude sea level signals associated with baroclinic pressure gradients. These signals evident in the tide gauge observations, are incorporated into the LAM through its open boundary forcing derived from a deep-water baroclinic ocean model (Bajo et al., 2019; Pringle et al., 2019).

Nevertheless, these differences emerged when comparing the accuracy of the two modelling approaches in reproducing the full time series of residual water levels, which, aside from storm surge events, is largely dominated by low-magnitude variability. The validation of the BSM's residual water levels against observations (Tables 2 and 5), however, yields RMSE values within 0.12 m, consistent with previous validations of similar basin scale storm surge models over the North Atlantic (Vousdoukas et al., 2016).

When the evaluation is focused on the capability in reproducing extreme events, which is the primary focus of the present study, the BSM outperforms the LAM in simulating the distribution of storm surges (Table 4), with further improvements observed following calibration (Table 6). These results reinforce the capability of the BSM, driven solely by atmospheric forcing, to accurately simulate storm surges and their climatological characteristics.

The wind drag coefficient (C_d) is essential for accurately modelling momentum transfer from the atmosphere to the ocean surface, particularly during storms (Moon et al., 2009). Although a coefficient of 0.0025 performs well, higher values may improve predictions of storm surges by better capturing strong wind effects (Marcos et al., 2009). Similarly, the bottom friction coefficient (C_b) affects energy dissipation as surges travel across the seabed, especially in shallow areas like Sligo, where bottom friction could be an equally dominant force (WMO, 2011). While increasing friction can overly dampen surge heights, lower values may enhance model accuracy for extreme events (WMO, 2011).

Thus, an iterative calibration procedure employed via trial-and-error approach, testing different combinations of wind drag and bottom friction coefficients showed improvements in the accuracy of the return levels (Table 6). The effectiveness of this process depends on a robust set of validation data, including historical extreme events, to ensure that the model improvements are meaningful. Q-Q plots, Taylor diagrams, and Skill Scores could be effectively used to identify optimal model parameters. While skill scores of the surges (residual water levels above

thresholds) were additionally considered for testing a set of near optimal calibration runs in this research, focusing solely on skill scores for the whole residual water level time series may also be sufficient (Warner et al., 2005; Zhong et al., 2010; Zhang et al., 2012; Ding et al., 2020). Furthermore, there are different sets of parameter values (for the C_d and C_b) yielding similar skill scores of the residual water levels and this fact is also evident from the Taylor Diagram (Fig. 7) suggesting that the model provide reliable solutions to small changes in the C_d and C_b values within certain ranges. This was also apparent from the calibration procedure where the C_d was varied by keeping the C_b constant and vice versa (see Appendix Figure A6 and Figure A7). Thus, certain combinations of the parameters (specifically varying both C_d and C_b) were found to yield similar model performance. Several simulations, such as SIM 7, SIM 8, and SIM 9 (see Appendix Table A2), show nearly identical skill scores despite differences in C_d and C_b values. This suggests that the model is not highly sensitive to parameter changes within specific ranges in this case. The model demonstrates comparable skill scores across a range of parameter configurations, highlighting the challenge of discerning unique parameter values for calibration. Further elaboration on this matter is beyond the scope of this paper. But in the context of the present research, as model performance to accurately simulate climatological data like return levels is the main priority, calibration is seen to have an impact on such simulations. Given that more than a decade of observational data is available for the study site, evaluation through Q-Q plots and extreme value analysis facilitated with the accuracy evaluation of different calibration runs. For instance, the calibration runs for both 0.005 & 0.005 and 0.005 & 0.0075 for 2020 yield similar values of skill scores for the residual water levels, i.e., 0.894 and 0.898 respectively (see Appendix Table A2), but on examining the modelled hindcasts through Q-Q plots and return levels by fitting extreme value models, better model performance was found for the latter. It is however acknowledged that limitations in spatial and temporal extent of the observations can limit such analysis. Numerical simulation of surges using such a large basin scale domain can be computationally intensive, especially from the perspective of climate projection. Li et al. (2013) found that while the simulated storm surge is significantly affected by the variation of the domain size when the domain is relatively small. When the domain size is greater than a given threshold value, "threshold domain size", the simulated storm surge is not sensitive to the variation of the domain size. As long as the model domain is larger than the "threshold domain size", the model results are considered reasonable as the model error due to model domain size will be <5 %. Selection of such a "threshold domain size" was not undertaken in this research but could be important for storm surge studies in areas where tide-surge interaction is significant and requires imposing tidal constituents at open boundaries as commonly done for storm surge projection studies in the North Sea (Debernard et al., 2002; Woth et al., 2006; Sterl et al., 2009; Howard et al., 2010; Gaslikova et al., 2013). Too large a domain in such cases could make the simulations computationally too expensive and complex.

5. Conclusion and future work

In the present research, the ability of a barotropic finite element storm surge model implemented using SHYFEM over the entire North Atlantic (BSM) and driven solely by atmospheric forcing (excluding tidal components), to simulate storm surges within Donegal Bay has been examined.

To assess the potential influence on predictive performance, the BSM is compared against a locally confined configuration of SHYFEM (LAM) applied within the bay. The BSM exhibits superior performance in reproducing the observed storm surges and the associated return levels across all four tide gauge stations within Donegal Bay as opposed to the LAM. The accurate return levels reinforce the ability of the BSM to be used for the projection of future changes in important climatological quantities associated with sea level extremes, such as return levels, it however does not assess the skill of the model in capturing extreme event timing (which is not the focus of the present research but could be important for storm surge forecasting). The exclusion of direct tidal modelling does not have any impact on the accuracy of the storm surges as the tide-surge interaction is negligible and difference in the RMSE between the residual water level time series between LAM and the BSM is just within $\sim$3 cm. The LAM which is forced with well calibrated data at its open boundary shows slightly better performance in reproducing the observed residual water level time series as it contains low-frequency and amplitude sea level components which cannot be reproduced by the BSM exclusively forced by atmospheric forcings. The BSM outperforms the LAM in reproducing the climatological statistics of the storm surges. Varying the wind drag and bottom friction coefficients for the BSM showed improvements not only in the hindcasts of the residual water levels but also in the accuracy of the storm surge return levels. Here, only one atmospheric dataset was used, and the performance of the BSM with different atmospheric datasets remain to be seen. Subject to the availability of observational data, model evaluation through Q-Q plots and climatological statistics, such as return levels, have proven valuable in assessing the suitability of a storm surge model for projecting climatological statistics thus proving its suitability to be used within climate projection studies. Additionally, such validation methods can aid in selecting an optimal set of calibration parameters, as error metrics can yield similar values across different parameter configurations, as observed in our case with just one year of validation data. This approach is particularly relevant for applications like the creation of flood risk maps, which is the next step of our research based on climatological statistics like return levels derived from forcing the BSM with atmospheric forcings from the outputs of climate models.

In conclusion, the BSM has proven to be well suited for projecting storm surges under climate scenarios for the northwest of Ireland when driven exclusively by atmospheric forcings and without the inclusion of tides. The present work in addition to addressing the research gaps for the northwest Ireland adds knowledge to the current state of the art BSM storm surge modelling approaches worldwide in terms of model setup and validation techniques. For regions with significant tide-surge interaction, where imposing tidal constituents at the open boundaries could be essential, selecting a "threshold domain size" could be a consideration as too big a domain could be computationally expensive for storm surge climate projection studies. In a subsequent paper, the projected storm surges will be combined with tidal components and projected mean sea level changes to estimate ESLs, from which return levels will be derived using extreme value statistics. This approach will facilitate the development of high-resolution flood risk maps for Donegal Bay, an underrepresented area where such maps are urgently needed to address vulnerability to the increasing risk from coastal flooding under future climate scenarios.

CRediT authorship contribution statement

Tasneem Ahmed: Writing – review & editing, Writing – original draft, Visualization, Validation, Software, Resources, Methodology, Investigation, Formal analysis, Data curation, Conceptualization. **Andrea Cucco:** Writing – review & editing, Writing – original draft, Visualization, Validation, Supervision, Software, Resources, Project administration, Methodology, Investigation, Formal analysis, Data curation, Conceptualization. **Giovanni Quattrocchi:** Writing – review & editing, Writing – original draft, Validation, Supervision, Formal analysis, Data curation. **Leo Creedon:** Writing – review & editing, Writing – original draft, Visualization, Validation, Supervision, Resources, Methodology, Investigation, Funding acquisition, Conceptualization. **Iulia Anton:** Writing – original draft, Validation, Software, Methodology, Investigation, Formal analysis, Data curation. **Michele Bendoni:** Writing – review & editing, Validation, Methodology, Conceptualization. **Stefano Taddei:** Writing – review & editing, Conceptualization. **Carlo Brandini:** Writing – original draft, Validation, Conceptualization. **Salem S Gharbia:** Writing – review & editing, Writing – original draft, Visualization, Validation, Supervision, Software, Resources, Project administration, Methodology, Investigation, Funding acquisition, Formal analysis, Data curation, Conceptualization.

Declaration of competing interest

The authors declare that they have no known competing financial interests or personal relationships that could have appeared to influence the work reported in this paper.

Acknowledgements

This research received funding from the European Union's Horizon 2020 research and innovation program under grant agreement No. 101003534.

Appendix

A1 Quantification of tide-surge interaction

As the tidal regime in Donegal Bay is mesotidal, the non-linear interaction of the tides and surges (extremes) is explored through the methodology proposed by Dixon and Tawn (1994) to identify the existence of non-linear tide-surge interaction within the Bay, if any, that could contribute to potential errors in the accuracy of simulating storm surges pertaining to the non-inclusion of tides in the BSM. In this method the tidal range is divided into five equi-probable bands, such that there is an equal number of surges associated with the tides in each band. So, an observed surge has equal probability of falling into any one of the five bands. For negligible tide-surge interaction, where tide and surges can be assumed to be independent processes, the number of surges per tidal band expected to exceed a threshold, u, would be the same. Assuming a threshold,u,of 99.95 percentile of surge distribution and assuming the tide and surge to be independent processes, one would expect $\frac{nobs \times 0.0005}{5} = e$ observations above the threshold in each tidal band, where *nobs* is the number of hourly surge observations, but we observe N_i, $i = 1,\ldots,5$ hourly observations in each of the five tidal bands above the threshold u. The test for interaction can then be tested by using a standard χ^2 test statistic as

$$\chi^2 = \sum_{i=1}^{5} \frac{(\mathbf{N_i} - \mathbf{e})^2}{\mathbf{e}} \tag{A.1}$$

This test statistic is small when the observed number of extreme surges per tidal band is close to the number expected if the tide and surge are independent but is large when there is interaction between tide and surge. The value of the test statistic above which tide surge interaction can be considered to be significant for the extremes is the 95 % significance level of the test statistic, i.e., $\chi^2_{4,0.95} = 9.5$.

Here the tide surge interaction is evaluated using this methodology for thresholds at a number of commonly used percentiles like 99, and 99.95 and 99.99 percentiles for all the four tide gauges within the Bay for the entire observation period (Fig. A.1,Fig. A.2,Fig. A.3,Fig. A.4,Fig. A.5,Fig. A.6, Fig. A.7, Table A.1, Table A.2).

Table A.1
. Statistics used to evaluate performance of the modelled hourly surge outputs against the hourly surge observations from the tide gauges within Donegal Bay.

Error statics	Formulae
Root mean square error	$RMSE = \sqrt{\frac{1}{N}\sum_{i=1}^{N}(S_i - O_i)^2}$
Correlation	$R = \frac{\sum_{i=1}^{N}(S_i - \overline{S_i})(O_i - \overline{O_i})}{\sqrt{\sum_{i=1}^{N}(S_i - \overline{S_i})^2}\sqrt{\sum_{i=1}^{N}(O_i - \overline{O_i})^2}}$
Bias	$Bias = \sum_{i=1}^{N}\frac{1}{N}(S_i - O_i)$
Skill	$Skill = 1 - \frac{\sum \lvert X_{model} - X_{obs}\rvert^2}{\sum (\lvert X_{model} - \overline{X_{obs}}\rvert + \lvert X_{obs} - \overline{X_{obs}}\rvert)^2}$

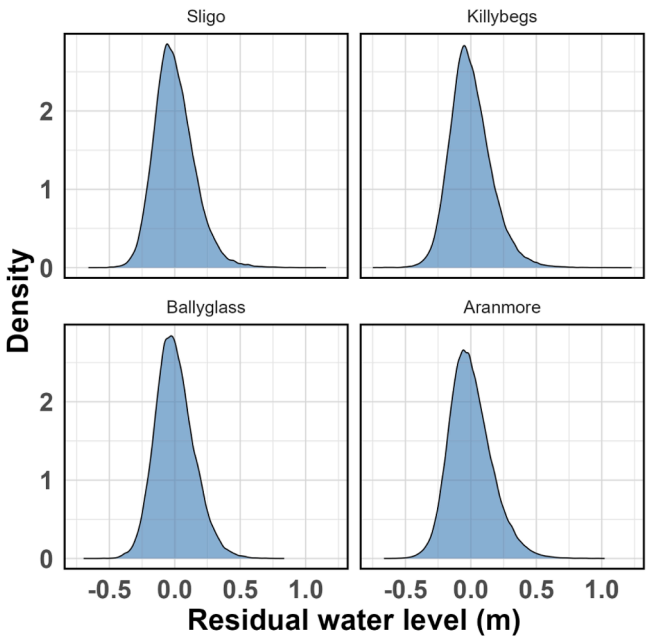

Fig. A.1. Distribution of residual water levels at the four Donegal Bay tide gauge stations (Sligo, Killybegs, Ballyglass, and Aranmore) are shown in the density plots along with the measure for skewness, standard deviation, and the interquartile range (IQR).

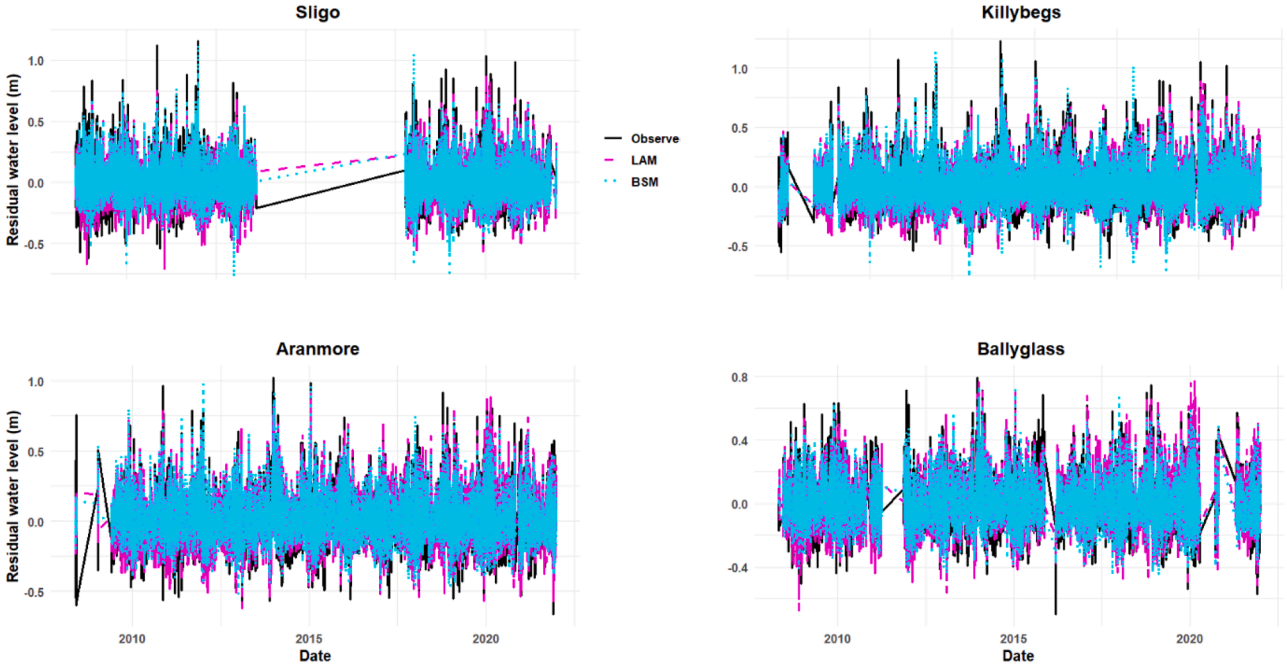

Fig. A.2. Time series of the observed and modelled residual water levels from the LAM and BSM at the four tide gauge stations for corresponding timestamps of the observed data at hourly frequency.

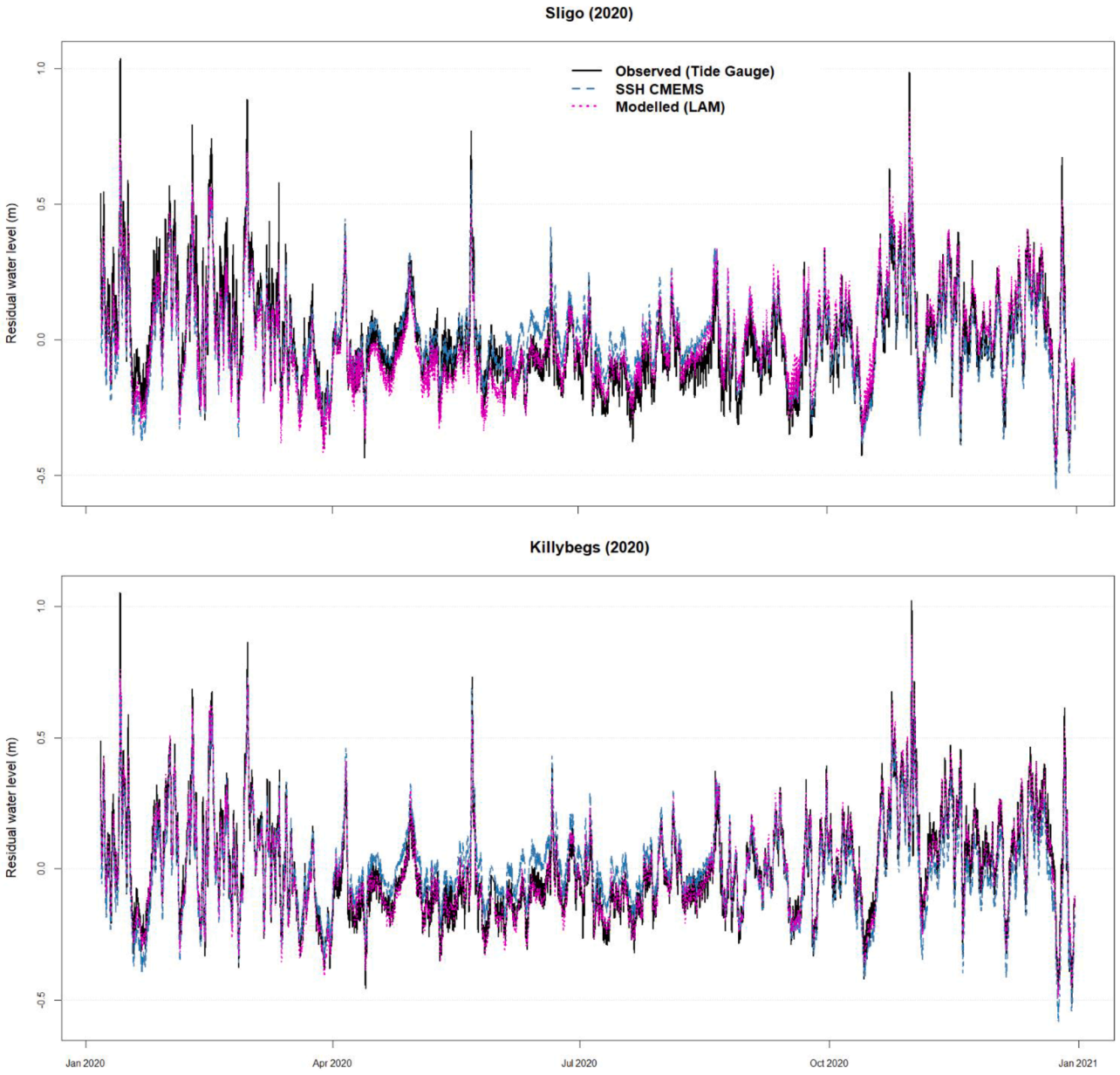

Fig. A.3. Comparison of the residual water levels between the observations (Sligo, Killybegs) with the residual water levels extracted from the CMEMS dataset, and that of the LAM outputs for the default calibration.

Table A.2
. Error statistics for the BSM total and filtered (>=0.5 m) time series of the residual water levels for the calibration runs for 2020 carried out by varying the wind drag (WD) coefficient (Cd) and keeping the bottom friction (BF) coefficient (Cb) constant and vice versa.

			Residual water level (m)				Filtered residual water level (>0.5 m)				Filtered residual water level (>0.75 m)			
ID	WD (C_d)	BF (C_b)	Corr	RMSE	Bias	**Skill**	Corr	RMSE	Bias	**Skill**	Corr	RMSE	BIAS	**Skill**
SIM 1	0.000001	0.0025	0.502	0.160	0.016	**0.699**	0.199	0.483	−0.462	**0.309**	−0.228	0.668	0.654	**0.205**
SIM 2	0.00001	0.0025	0.505	0.160	0.016	**0.700**	0.201	0.482	−0.461	**0.309**	−0.225	0.667	0.653	**0.205**
SIM 3	0.0001	0.0025	0.537	0.156	0.015	**0.711**	0.223	0.471	−0.451	**0.315**	−0.188	0.653	0.640	**0.208**
SIM 4	0.001	0.0025	0.749	0.126	0.014	**0.807**	0.445	0.364	−0.347	**0.380**	0.279	0.523	0.514	**0.249**
SIM 5	0.002	0.0025	0.818	0.108	0.017	**0.872**	0.578	0.258	−0.237	**0.485**	0.540	0.390	0.382	**0.314**
SIM 6	0.003	0.0025	0.819	0.108	−0.020	**0.891**	0.519	0.143	0.061	**0.658**	0.494	0.275	0.258	**0.415**
SIM 7	0.003	0.005	0.837	0.104	−0.026	**0.893**	0.499	0.160	0.093	**0.617**	0.524	0.292	0.280	**0.392**
SIM 8	0.003	0.0075	0.841	0.104	−0.030	**0.890**	0.451	0.177	0.115	**0.591**	0.508	0.307	0.296	**0.377**
SIM 9	0.004	0.0025	0.813	0.118	−0.025	**0.888**	0.545	0.137	−0.053	**0.784**	0.545	0.178	0.141	**0.541**
SIM 10	0.004	0.005	0.841	0.107	−0.034	**0.900**	0.515	0.129	−0.007	**0.769**	0.587	0.194	0.176	**0.525**
SIM 11	0.004	0.0075	0.849	0.105	−0.038	**0.900**	0.457	0.137	0.025	**0.722**	0.574	0.215	0.200	**0.487**
SIM 12	0.005	0.0025	0.806	0.135	−0.031	**0.873**	0.541	0.206	−0.162	**0.725**	0.573	0.126	0.029	**0.744**
SIM 13	0.005	0.005	0.840	0.117	−0.041	**0.894**	0.502	0.165	−0.099	**0.786**	0.617	0.116	0.077	**0.739**

(*continued on next page*)

Table A.2 (*continued*)

			Residual water level (m)				Filtered residual water level (>0.5 m)				Filtered residual water level (>0.75 m)			
SIM 14	0.005	0.0075	0.850	0.113	−0.047	**0.898**	0.444	0.152	−0.059	**0.782**	0.597	0.135	0.109	**0.695**
SIM 15	0.006	0.0025	0.808	0.153	0.038	**0.857**	0.590	0.207	0.152	**0.603**	0.653	0.158	−0.082	**0.751**
SIM 16	0.007	0.0025	0.803	0.176	0.045	**0.834**	0.580	0.287	0.241	**0.490**	0.658	0.240	−0.186	**0.512**
SIM 17	0.008	0.0025	0.799	0.200	0.052	**0.811**	0.571	0.371	0.327	**0.408**	0.661	0.332	−0.288	**0.404**
SIM 18	0.009	0.0025	0.796	0.224	0.059	**0.788**	0.563	0.453	0.411	**0.346**	0.664	0.426	−0.386	**0.323**
SIM 19	0.01	0.0025	0.794	0.248	0.067	**0.766**	0.555	0.535	0.492	**0.301**	0.665	0.519	−0.482	**0.263**
SIM 20	0.0025	0.0001	0.741	0.130	−0.001	**0.860**	0.403	0.232	−0.176	**0.572**	0.557	0.361	0.315	**0.365**
SIM 21	0.0025	0.001	0.804	0.110	0.012	**0.883**	0.558	0.206	−0.175	**0.583**	0.572	0.324	0.3066	**0.369**
SIM 22	0.0025	0.0025	0.826	0.105	0.018	**0.888**	0.601	0.210	−0.185	**0.563**	0.585	0.329	0.318	**0.359**
SIM 23	0.0025	0.005	0.835	0.105	0.024	**0.885**	0.598	0.221	−0.197	**0.537**	0.575	0.344	0.335	**0.346**
SIM 24	0.0025	0.0075	0.834	0.106	0.027	**0.880**	0.577	0.231	−0.208	**0.521**	0.531	0.356	0.347	**0.337**
SIM 25	0.0025	0.01	0.829	0.108	0.029	**0.875**	0.553	0.239	−0.216	**0.510**	0.465	0.366	0.356	**0.331**

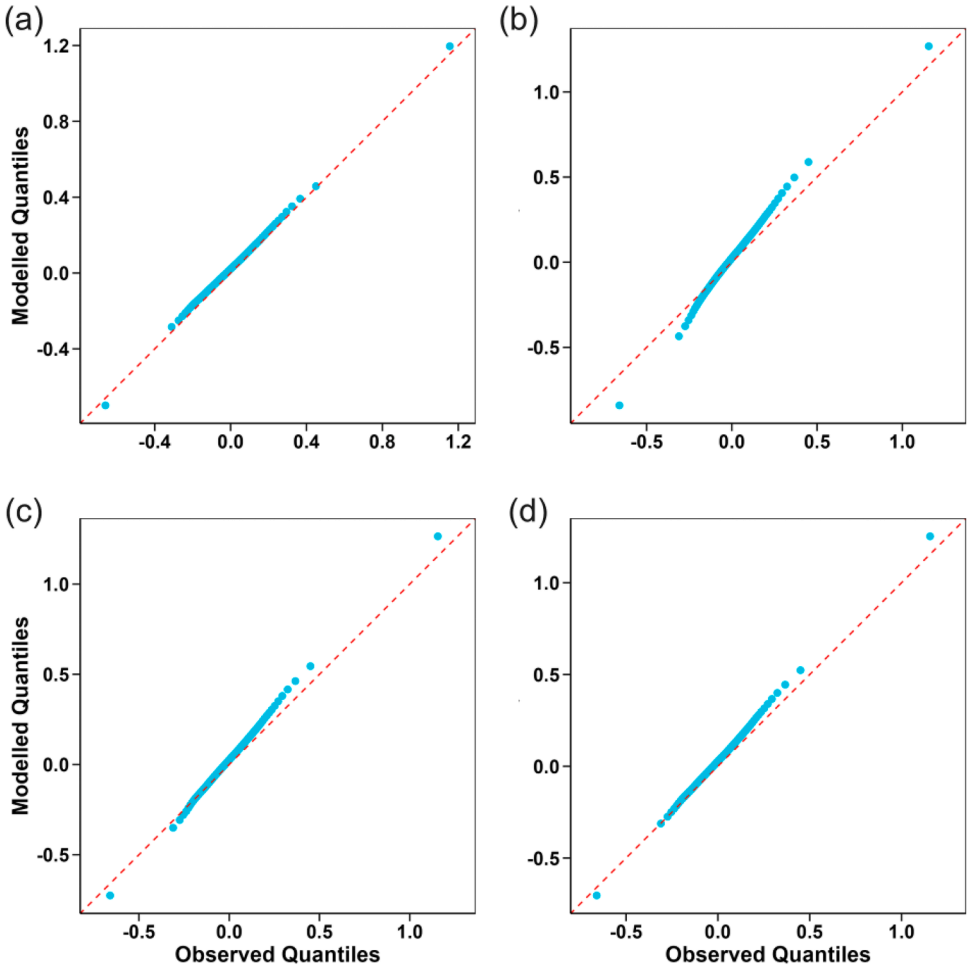

Fig. A.4. Q-Q plots of the Observed vs Modelled quantiles of the residual water levels for the BSM corresponding to calibration runs (a) 0.004 & 0.0075, (b) 0.005 & 0.0025, (c) 0.005 & 0.005, and (d) 0.005 & 0.0075 for C_d and C_b, respectively at the Sligo tide gauge.

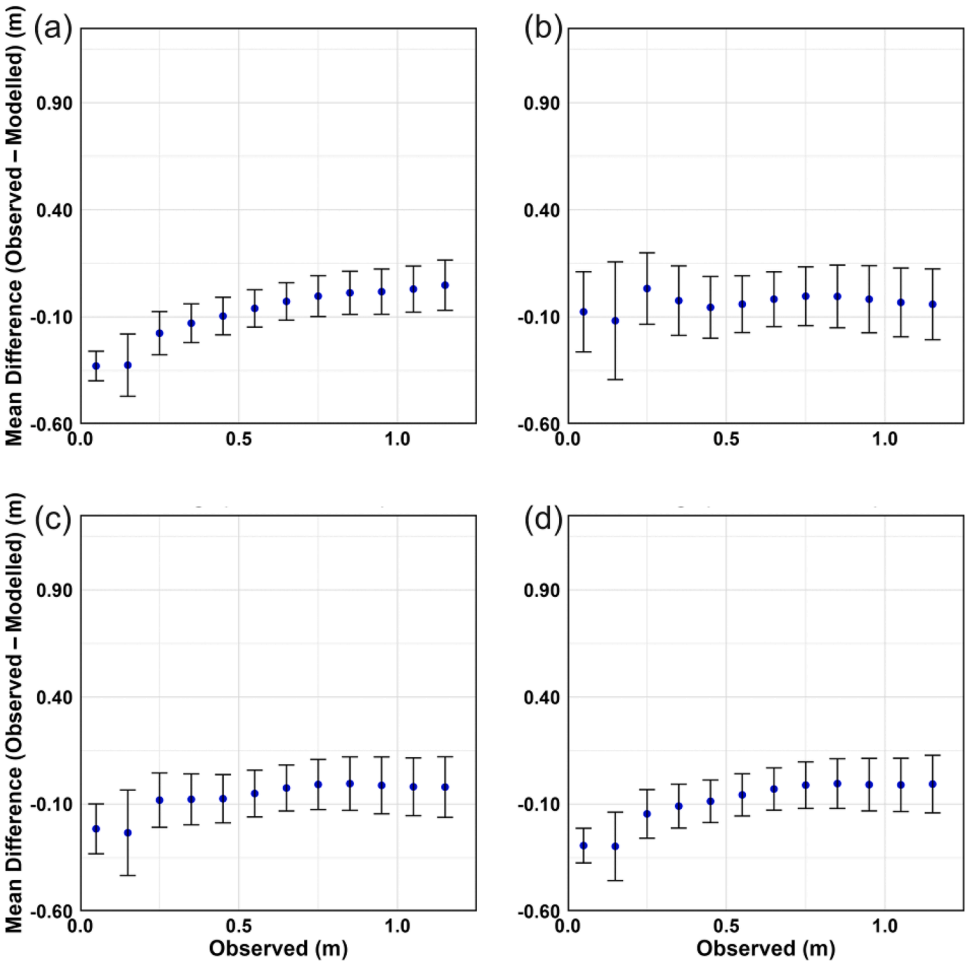

Fig. A.5. Mean difference plots for the BSM corresponding to calibration runs (a) 0.004 & 0.0075, (b) 0.005 & 0.0025, (c) 0.005 & 0.005, and (d) 0.005 & 0.0075 for C_d and C_b, respectively at the Sligo tide gauge.

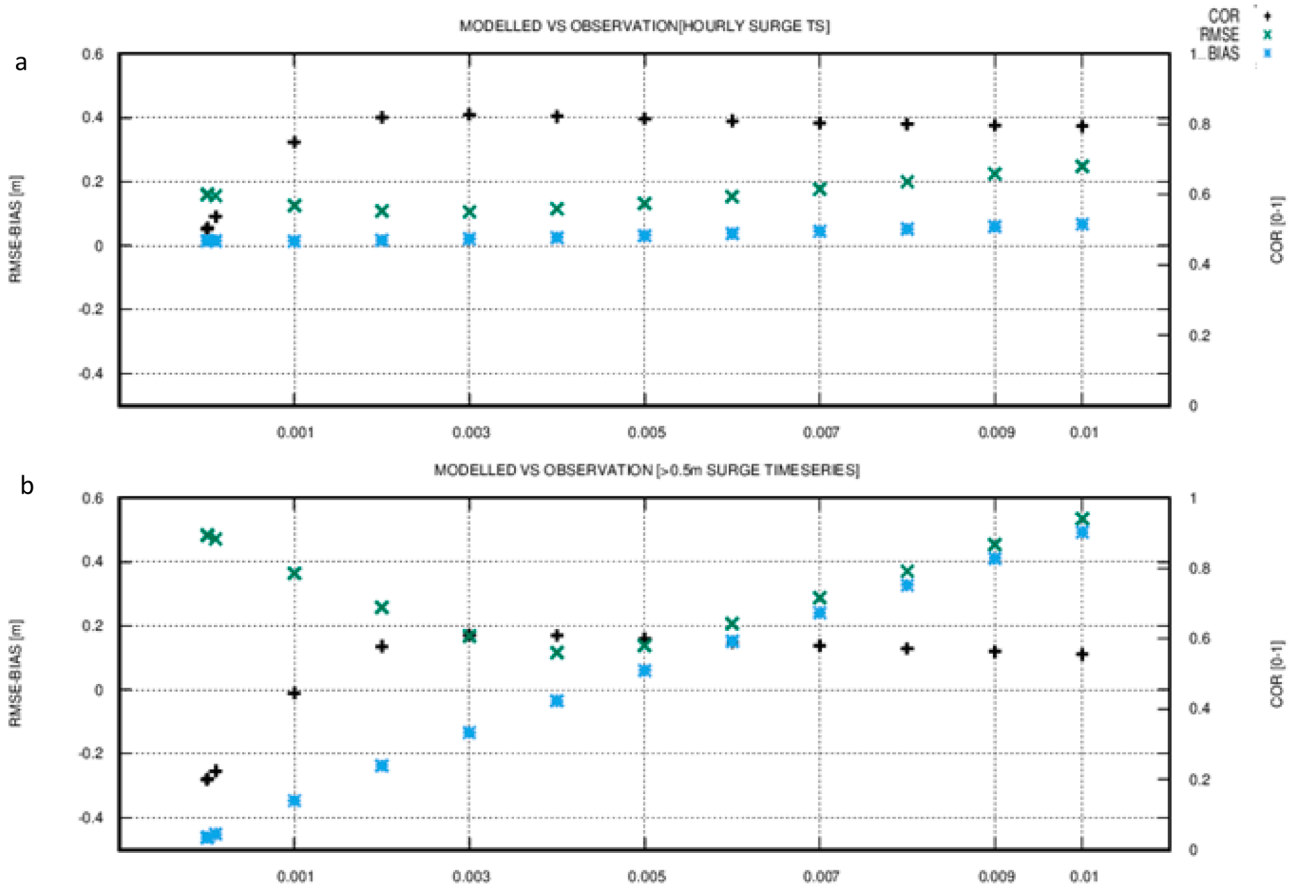

Fig. A.6. Error metrics for the BSM 2020 a) Total residual water level time series b) Filtered (>0.5 m) residual water level time series pertaining to the calibration runs where the wind drag coefficient (C_d) is varied keeping the bottom drag coefficient (C_b) at its default value (0.0025). The x axis represents dimensionless values of C_d.

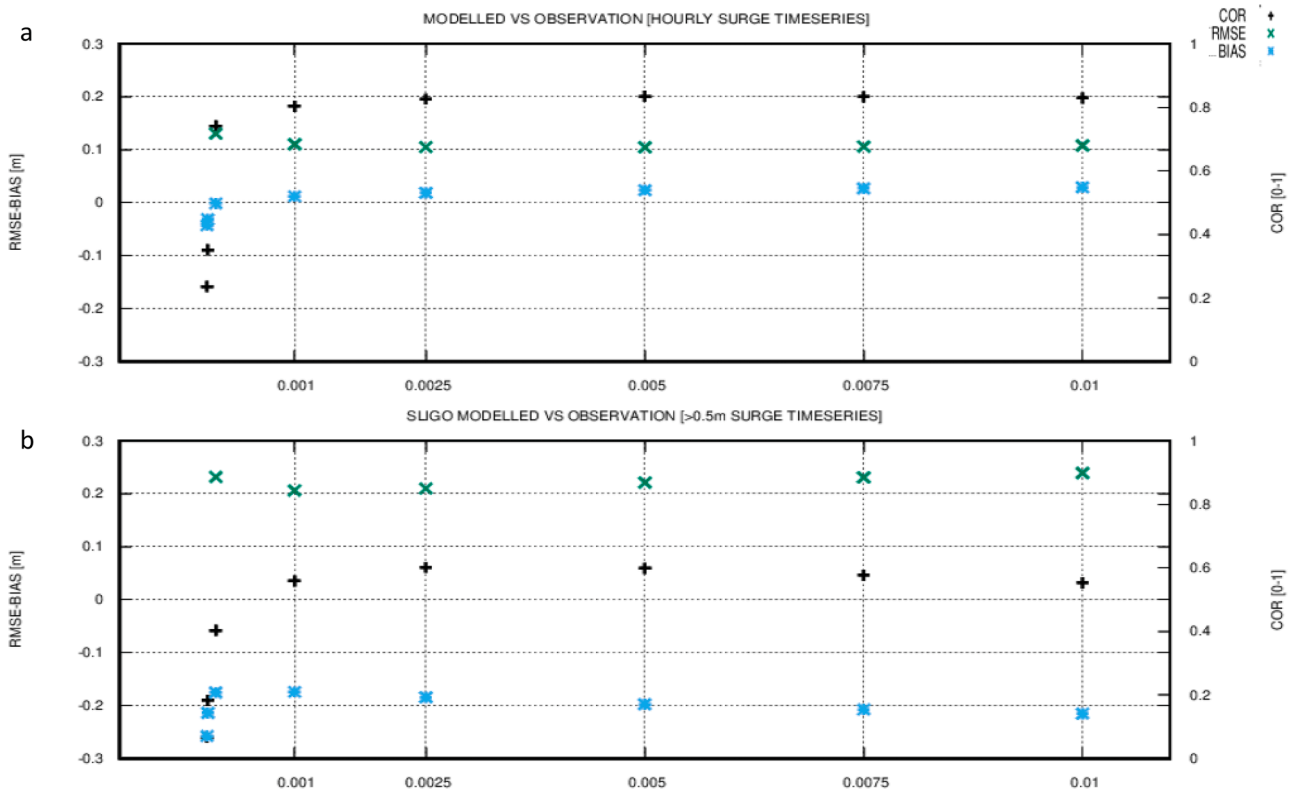

Fig. A.7. Error metrics for the BSM 2020 a) Total residual water level time series b) Filtered (>0.5 m) residual water level time series pertaining to the calibration runs where the bottom drag coefficient (Cb) is varied keeping the wind drag coefficient (Cd) at its default value (0.0025). The x axis represents dimensionless values of Cb.

Data availability

Data will be made available on request.

References

Androulidakis, Y.S., et al., 2015. Storm surges in the Mediterranean Sea: variability and trends under future climatic conditions. Dyn. Atmos. Oceans 71, 56–82. https://doi.org/10.1016/j.dynatmoce.2015.06.001. Available at.

Antony, C., et al., 2022. Sea-level extremes of meteorological origin in the Red Sea. Weather. Clim. Extrem. 35, 100409. https://doi.org/10.1016/j.wace.2022.100409. Available at.

Arns, A., et al., 2015. The impact of sea level rise on storm surge water levels in the northern part of the German Bight. Coast. Eng. 96, 118–131. https://doi.org/10.1016/j.coastaleng.2014.12.002. Available at.

Arpaia, L. et al. (2023) 'A flexible z -layers approach for the accurate representation of free surface flows in a coastal ocean model (SHYFEM v . 7 _ 5 _ 71)', pp. 6899–6919.

Bajo, M., et al., 2007. A finite element operational model for storm surge prediction in Venice. Estuar. Coast. Shelf. Sci. 75 (1–2), 236–249. https://doi.org/10.1016/j.ecss.2007.02.025. Available at.

Bajo, M., et al., 2019. Storm surge and seiche modelling in the Adriatic Sea and the impact of data assimilation. Quart. J. R. Meteorol. Soc. 145 (722), 2070–2084. https://doi.org/10.1002/qj.3544. Available at.

Bajo, M. et al. (2023) 'Modelling the barotropic sea level in the Mediterranean Sea using data assimilation', pp. 559–579.

Bernier, N.B., et al., 2007. Mapping the return periods of extreme sea levels: allowing for short sea level records, seasonality, and climate change. Glob. Planet. Change 57 (1–2), 139–150. https://doi.org/10.1016/j.gloplacha.2006.11.027. Available at.

Blain, C.A., Westerink, J.J., Luettich, R.A., 1994. The influence of domain size on the response characteristics of a hurricane storm model. J. Geophys. Res. 99 (C9), 18467–18479. https://doi.org/10.1029/94JC01348.

Bloemendaal, N., et al., 2019. Global modeling of tropical cyclone storm surges using high-resolution forecasts. Clim. Dyn. 52 (7–8), 5031–5044. https://doi.org/10.1007/s00382-018-4430-x. Available at.

Brown, J.M., Souza, A.J., Wolf, J., 2010a. An 11-year validation of wave-surge modelling in the Irish Sea, using a nested POLCOMS-WAM modelling system. Ocean. Model. (Oxf.) 33 (1–2), 118–128. https://doi.org/10.1016/j.ocemod.2009.12.006. Available at.

Brown, J.M., Souza, A.J., Wolf, J., 2010b. An investigation of recent decadal-scale storm events in the eastern Irish sea. J. Geophys. Res. 115 (5), 1–12. https://doi.org/10.1029/2009JC005662. Available at.

Calafat, F.M., et al., 2014. The ability of a barotropic model to simulate sea level extremes of meteorological origin in the Mediterranean Sea, including those caused by explosive cyclones. J. Geophys. Res. 119 (11), 7840–7853. https://doi.org/10.1002/2014JC010360. Available at.

Campos-Caba, R. et al. (2024) 'Assessing the storm surge model performance: what error indicators can measure the skill?', (May), pp. 1–27.

Chen, W., 2022. Typhoon wave simulation responses to various reanalysis wind fields and computational domain sizes. J. Mar. Sci. Eng. 10 (10), 1360. https://doi.org/10.3390/jmse10101360. Available at.

Cid, A., et al., 2016. Long - term changes in the frequency, intensity and duration of extreme storm surge events in southern Europe'. Clim. Dyn. 46 (5), 1503–1516. https://doi.org/10.1007/s00382-015-2659-1. Available at.

Coles, S. (2001) An introduction to statistical modeling of extreme values, the effects of brief mindfulness intervention on acute pain experience: an examination of individual difference. London: Springer London (Springer Series in Statistics). Available at: https://doi.org/10.1007/978-1-4471-3675-0.

Conte, D., Lionello, P., 2013. Characteristics of large positive and negative surges in the Mediterranean Sea and their attenuation in future climate scenarios. Glob. Planet. Change 111, 159–173. https://doi.org/10.1016/j.gloplacha.2013.09.006. Available at.

Cooper, J.A.G., et al., 2004. Identifying storm impacts on an embayed, high-energy coastline : examples from western Ireland'. Mar. Geol. 210 (1–4), 261–280. https://doi.org/10.1016/j.margeo.2004.05.012. Available at.

Copernicus Marine Service (2020) 'IBI PHY-MY for Atlantic -Iberian Biscay Irish- Ocean physics reanalysis product', (September), pp. 1–50. Available at: https://doi.org/10.48670/moi-00029.

Costa, W., et al., 2023. A regional analysis of tide-surge interactions during extreme water levels in complex coastal systems of Aotearoa New Zealand. Front. Mar. Sci. 10 (May), 1–21. https://doi.org/10.3389/fmars.2023.1170756. Available at.

Cucco, A., et al., 2016. Hydrodynamic modelling of coastal seas: the role of tidal dynamics in the Messina Strait, Western Mediterranean Sea. Nat. Haz. Earth Syst. Sci. 16 (7), 1553–1569. https://doi.org/10.5194/nhess-16-1553-2016. Available at.

Cucco, A., et al., 2023. Assessing the risk of oil spill impacts and potential biodiversity loss for coastal marine environment at the turn of the COVID-19 pandemic event. Sci. Total Environ. 894 (February), 164972. https://doi.org/10.1016/j.scitotenv.2023.164972. Available at.

Cucco, A., et al., 2024. Operational oceanography in ports and coastal areas, applications for the management of pollution events. J. Mar. Sci. Eng. 12 (3). https://doi.org/10.3390/jmse12030380. Available at.
Cucco, A., Umgiesser, G., 2006. Modeling the Venice Lagoon residence time. Ecol. Modell. 193, 34–51. https://doi.org/10.1016/j.ecolmodel.2005.07.043, 1-2 SPEC. ISS.Available at.
Debernard, J., Sætra, Ø., Røed, L., 2002. Future wind, wave and storm surge climate in the northern North Atlantic. Clim. Res. 23 (1), 39–49. https://doi.org/10.3354/cr023039. Available at.
Ding, Y., et al., 2020. Simulation and {prediction} of {storm} {surges} and {waves} {using} a {fully} {integrated} {process} {model} and a {parametric} {cyclonic} {wind} {model}. J. Geophys. Res. 125 (7). https://doi.org/10.1029/2019JC015793. Available at.
Dixon, M.J., Tawn, J.A., 1994. Extreme Sea-levels at the UK a-class sites: site– by-site analysis. Pol. Internal Document 65 [Preprint], (65).
Dullaart, J.C.M., et al., 2020. Advancing global storm surge modelling using the new ERA5 climate reanalysis. Clim. Dyn. 54 (1–2), 1007–1021. https://doi.org/10.1007/s00382-019-05044-0. Available at.
Elsäßer, B. (2010) 'Storm surge hind- and forecasting using Mike21FM - simulation of surges around the Irish Coast', (January).
Federico, I., et al., 2017. Coastal ocean forecasting with an unstructured grid model in the southern Adriatic and northern Ionian seas. Nat. Haz. Earth Syst. Sci. 17 (1), 45–59. https://doi.org/10.5194/nhess-17-45-2017. Available at.
Feng, J., et al., 2021. Comparison between the skew surge and residual water level along the coastline of China. J. Hydrol. 598, 126299. https://doi.org/10.1016/j.jhydrol.2021.126299. November 2020Available at.
Fernández-Montblanc, T., et al., 2019. Towards robust pan-European storm surge forecasting. Ocean. Model. (Oxf.) 133, 129–144. https://doi.org/10.1016/j.ocemod.2018.12.001. Available at.
Ferrarin, C., et al., 2013. Tide-surge-wave modelling and forecasting in the Mediterranean Sea with focus on the Italian coast. Ocean. Model. (Oxf.) 61, 38–48. https://doi.org/10.1016/j.ocemod.2012.10.003. Available at.
Ferrarin, C., et al., 2019. Cross-scale operational oceanography in the Adriatic Sea. J. Oper. Ocean. 12 (2), 86–103. https://doi.org/10.1080/1755876X.2019.1576275. Available at.
Ferrarin, C., et al., 2023. Sea level and temperature extremes in a regulated lagoon of Venice. Front. Clim. 5. https://doi.org/10.3389/fclim.2023.1330388. January 2022). Available at.
Ferrarin, C., Umgiesser, G., 2005. Hydrodynamic modeling of a coastal lagoon: the Cabras lagoon in Sardinia, Italy. Ecol. Modell. 188 (2–4), 340–357. https://doi.org/10.1016/j.ecolmodel.2005.01.061. Available at.
Gaslikova, L., Grabemann, I., Groll, N., 2013. Changes in North Sea storm surge conditions for four transient future climate realizations. Nat. Haz. 66 (3), 1501–1518. https://doi.org/10.1007/s11069-012-0279-1. Available at.
Geuzaine, C., Remacle, J., 2009. Gmsh: a 3-D finite element mesh generator with built-in pre- and post-processing facilities. Int. J. Numer. Methods Eng. 79 (11), 1309–1331. https://doi.org/10.1002/nme.2579. Available at.
Gilleland, E., Katz, R.W., 2016. ExtRemes 2.0: an extreme value analysis package in R. J. Stat. Softw. https://doi.org/10.18637/jss.v072.i08. Available at.
Greatbatch, R.J., Lu, Y., de Young, B., 1996. Application of a barotropic model to North Atlantic synoptic sea level variability. J. Mar. Res. 54 (3), 451–469. Available atelischolar.library.yale.edu/journal_of_marine_research/2187.
Group, G.C. (2022) 'The GEBCO_2022 Grid - a continuous terrain model of the global oceans and land.' NERC EDS British Oceanographic Data Centre NOC. Available at: 10.5285/e0f0bb80-ab44-2739-e053-6c86abc0289c.
Haigh, I., Nicholls, R., Wells, N., 2010. Assessing changes in extreme sea levels: application to the English Channel, 1900-2006'. Cont. Shelf. Res. 30 (9), 1042–1055. https://doi.org/10.1016/j.csr.2010.02.002. Available at.
Howard, T., 2022. Technical note: tail behaviour of the statistical distribution of extreme storm surges. Ocean Science 18 (3), 905–913. https://doi.org/10.5194/os-18-905-2022. Available at.
Howard, T., Lowe, J., Horsburgh, K., 2010. Interpreting century-scale changes in southern north sea storm surge climate derived from coupled model simulations. J. Clim. 23 (23), 6234–6247. https://doi.org/10.1175/2010JCLI3520.1. Available at.
INFOMAR (2024) Data access and download. Available at: https://www.infomar.ie/data.
Jensen, T.G., 1998. Open boundary conditions in stratified ocean models. J. Mar. Syst. 16 (3–4), 297–322. https://doi.org/10.1016/S0924-7963(97)00023-7. Available at.
Kelley, D.E. (2018) Oceanographic analysis with R, Oceanographic analysis with R. New York, NY: springer New York. Available at: https://doi.org/10.1007/978-1-4939-8844-0.
Kerr, P.C., et al., 2013. U.S. IOOS coastal and ocean modeling testbed: inter-model evaluation of tides, waves, and hurricane surge in the Gulf of Mexico. J. Geophys. Res. 118 (10), 5129–5172. https://doi.org/10.1002/jgrc.20376. Available at.
Kim, J., et al., 2021. Numerical analysis of storm surges on Canada's western Arctic coastline. J. Mar. Sci. Eng. 9 (3), 326. https://doi.org/10.3390/jmse9030326. Available at.
Kirstensen, N.M., et al., 2024. NORA-surge : a storm surge hindcast for the Norwegian Sea, the North Sea and the Barents Sea'. Ocean. Model. (Oxf.) 191, 102406. https://doi.org/10.1016/j.ocemod.2024.102406. December 2023Available at.
Lagomarsino-Oneto, D., et al., 2024. Unraveling the non-homogeneous dispersion processes in ocean and coastal circulations using a clustering approach. Geophys. Res. Lett. 51 (9). https://doi.org/10.1029/2023GL107900. Available at.
Laino, E., Iglesias, G., 2024a. High - Level Characterisation and Mapping of Key Climate - Change Hazards in European Coastal Cities, Natural Hazards. Springer, Netherlands. https://doi.org/10.1007/s11069-023-06349-4. Available at.
Laino, E., Iglesias, G., 2024b. Multi-hazard assessment of climate-related hazards for European coastal cities. J. Environ. Manage. 357 (March), 120787. https://doi.org/10.1016/j.jenvman.2024.120787. Available at.
Li, R., et al., 2013. On the sensitivity of hurricane storm surge simulation to domain size. Ocean. Model. (Oxf.) 67, 1–12. https://doi.org/10.1016/j.ocemod.2013.03.005. Available at.
Liao, Y.P., Kaihatu, J.M., 2016. The effect of wind variability and domain size in the Persian Gulf on predicting nearshore wave energy near Doha, Qatar. Appl. Ocean Res. 55, 18–36. https://doi.org/10.1016/j.apor.2015.11.012. Available at.
Lin, N., et al., 2010. Risk assessment of hurricane storm surge for New York City. J. Geophys. Res. Atmos. 115 (18), 1–11. https://doi.org/10.1029/2009JD013630. Available at.
Lionello, P., Galati, M.B., Elvini, E., 2012. Extreme storm surge and wind wave climate scenario simulations at the Venetian littoral. Phys. Chem. Earth 86–92. https://doi.org/10.1016/j.pce.2010.04.001, 40–41Available at.
Macpherson, L.R., et al., 2022. Incorporating historical information to improve extreme sea level estimates. Nat. Haz. Earth Syst. Sci. (Jan.) 1–23. https://doi.org/10.5194/nhess-2021-406. Available at.
Marcos, M., et al., 2011. Changes in storm surges in southern Europe from a regional model under climate change scenarios. Glob. Planet. Change 77 (3–4), 116–128. https://doi.org/10.1016/j.gloplacha.2011.04.002. Available at.
Marcos, M., et al., 2012. Effect of sea level extremes on the western Basque coast during the 21st century. Clim. Res. 51 (3), 237–248. https://doi.org/10.3354/cr01069. Available at.
Marcos, M., Tsimplis, M.N., Shaw, A.G.P., 2009. Sea level extremes in southern Europe. J. Geophys. Res. 114 (1), 1–16. https://doi.org/10.1029/2008JC004912. Available at.
Mel, R., Sterl, A., Lionello, P., 2013. High resolution climate projection of storm surge at the Venetian coast. Nat. Haz. Earth Syst. Sci. 13 (4), 1135–1142. https://doi.org/10.5194/nhess-13-1135-2013. Available at.
Moon, I.J., et al., 2009. Effect of the surface wind stress parameterization on the storm surge modeling. Ocean. Model. (Oxf.) 29 (2), 115–127. https://doi.org/10.1016/j.ocemod.2009.03.006. Available at.
Morey, S.L., et al., 2006. Remote forcing contribution to storm-induced sea level rise during Hurricane Dennis. Geophys. Res. Lett. 33 (19), 1–5. https://doi.org/10.1029/2006GL027021. Available at.
Muis, S., et al., 2016. A global reanalysis of storm surges and extreme sea levels. Nat. Commun. https://doi.org/10.1038/ncomms11969, 7(May). Available at.
O'Brien, L., et al., 2018. Catalogue of extreme wave events in Ireland: revised and updated for 14 680 BP to 2017. Nat. Haz. Earth Syst. Sci. 18 (3), 729–758. https://doi.org/10.5194/nhess-18-729-2018. Available at.
Olbert, A.I., et al., 2013. Tide-surge interactions and their effects on total sea levels in Irish coastal waters. Ocean. Dyn. 63 (6), 599–614. https://doi.org/10.1007/s10236-013-0618-0. Available at.
Olbert, A.I., Hartnett, M., 2010. Storms and surges in Irish coastal waters. Ocean. Model. (Oxf.) 34 (1–2), 50–62. https://doi.org/10.1016/j.ocemod.2010.04.004. Available at.
OPW, 2020. Irish Coastal Wave and water level Modelling Study 2018: phase 1 - extreme water levels', (December). Available at https://s3-eu-west-1.amazonaws.com/docs.floodinfo.opw/floodinfo_docs/ICWWS-2018/Phase-1/IBE1505_ICWWS_Ph1_Rp01_F02.pdf.
Park, K., et al., 2022. The contribution of hurricane remote ocean forcing to storm surge along the southeastern U.S. coast. Coast. Eng. 173, 104098. https://doi.org/10.1016/j.coastaleng.2022.104098. October 2021Available at.
Pavlova, A., et al., 2022. Storm surges and extreme wind waves in the Caspian Sea in the present and future climate. Civ. Eng. J. (Iran) 8 (11), 2353–2377. https://doi.org/10.28991/CEJ-2022-08-11-01. Available at.
Pinheiro, J.P., et al., 2020. Tide-surge interaction in Ria de Aveiro lagoon and its influence in local inundation patterns. Cont. Shelf. Res. 200. https://doi.org/10.1016/j.csr.2020.104132. October 2019). Available at.
Pringle, W.J. et al. (2019) 'Baroclinic coupling improves depth-integrated modeling of coastal sea level variations around Puerto Rico and the U . S . Virgin Islands Journal of Geophysical Research : oceans', pp. 2196–2217. Available at: https://doi.org/10.1029/2018JC014682.
Pugh, D., Woodworth, P., 2014. Sea-Level Science. 1st Edn. Cambridge University Press. https://doi.org/10.1017/CBO9781139235778. Available at.
Rahmstorf, S., 2017. Rising hazard of storm-surge flooding. Proc. Natl. Acad. Sci. U.S.A. 114 (45), 11806–11808. https://doi.org/10.1073/pnas.1715895114. Available at.
Ratsimandresey, A.W., et al., 2008. A 44-year (1958-2001) sea level residual hindcast over the Mediterranean Basin. Phys. Chem. Earth 33 (3–4), 250–259. https://doi.org/10.1016/j.pce.2007.02.002. Available at.
Resio, D.T., Westerink, J.J., 2008. Modeling the physics of storm surges. Phys. Today 61 (9), 33–38. https://doi.org/10.1063/1.2982120. Available at.
Roberts, C.D., et al., 2018. Climate model configurations of the ecmwf integrated forecasting system (ecmwf-ifs cycle 43r1) for highresmip. Geosci. Model. Dev. 11 (9), 3681–3712. https://doi.org/10.5194/gmd-11-3681-2018. Available at.
Roland, A., et al., 2009. On the development and verification of a 2-D coupled wave-current model on unstructured meshes. J. Mar. Syst. 78, S244–S254. https://doi.org/10.1016/j.jmarsys.2009.01.026. SUPPL. 1Available at.
Sannino, G., et al., 2022. Modelling Present and Future Climate in the Mediterranean Sea: a Focus on Sea-Level change, Climate Dynamics. Springer, Berlin Heidelberg. https://doi.org/10.1007/s00382-021-06132-w. Available at.

Stephenson, A. (2017) 'Harmonic analysis of tides using TideHarmonics', 180(1), pp. 1–17.
Sardana, D., Kumar, P., Rajni, 2024. CMIP6 model evaluation for sea surface height responses to ENSO. Clim. Dyn. 62 (3), 1829–1847. https://doi.org/10.1007/s00382-023-06997-z.
Sterl, A., et al., 2009. An ensemble study of extreme storm surge related water levels in the North Sea in a changing climate. Ocean Science 5 (3), 369–378. https://doi.org/10.5194/os-5-369-2009. Available at.
Taylor, K.E., 2001. Summarizing multiple aspects of model performance in a single diagram. J. Geophys. Res. 106 (D7), 7183–7192. https://doi.org/10.1029/2000JD900719. Available at.
Team, R.C. (2023) 'R: A Language and Environment for Statistical Computing'. Vienna, Austria: R Foundation for Statistical Computing. Available at: https://www.r-project.org/.
Tiwari, A., et al., 2025. Public perceptions of climate risks, vulnerability, and adaptation strategies: fuzzy cognitive mapping in Irish and Spanish living labs. Environ. Sustain. Indicat. 26 (March), 100678. https://doi.org/10.1016/j.indic.2025.100678. Available at.
Tsimplis, M.N., Blackman, D., 1997. Extreme sea-level distribution and return periods in the Aegean and Ionian Seas. Estuar. Coast. Shelf. Sci. 44 (1), 79–89. https://doi.org/10.1006/ecss.1996.0126. Available at.
Umgiesser, G., et al., 2004. A finite element model for the Venice Lagoon. Development, set up, calibration and validation. J. Mar. Syst. 51, 123–145. https://doi.org/10.1016/j.jmarsys.2004.05.009, 1-4 SPEC. ISS.Available at.
Umgiesser, G., et al., 2021. The prediction of floods in Venice: methods, models and uncertainty (review article). Nat. Haz. Earth Syst. Sci. 21 (8), 2679–2704. https://doi.org/10.5194/nhess-21-2679-2021. Available at.
Vousdoukas, M.I., et al., 2016. Projections of extreme storm surge levels along Europe. Clim. Dyn. 47 (9–10), 3171–3190. https://doi.org/10.1007/s00382-016-3019-5. Available at.
Wang, S. et al. (2008) The impact of climate change on storm surges over Irish waters.
Warner, J.C., Geyer, W.R., Lerczak, J.A., 2005. Numerical modeling of an estuary: a comprehensive skill assessment. J. Geophys. Res. 110 (5), 1–13. https://doi.org/10.1029/2004JC002691. Available at.
Wessel, P., Smith, W.H.F., 1996. A global, self-consistent, hierarchical, high-resolution shoreline database. J. Geophys. Res. 101 (4), 8741–8743. https://doi.org/10.1029/96jb00104. Available at.
Wilk, M.B., Gnanadesikan, R., 1968. Probability plotting methods for the analysis of data. Biometrika 55 (1), 1. https://doi.org/10.2307/2334448. Available at.
Williams, J., et al., 2016. Tide and skew surge independence: new insights for flood risk. Geophys. Res. Lett. 43 (12), 6410–6417. https://doi.org/10.1002/2016GL069522. Available at.
WMO, 2011. Guide to Storm Surge forecasting. 2011 ed. World Meteorological Organization, Geneva, Switzerland.
Woth, K., Weisse, R., Von Storch, H., 2006. Climate change and North Sea storm surge extremes: an ensemble study of storm surge extremes expected in a changed climate projected by four different regional climate models. Ocean. Dyn. 56 (1), 3–15. https://doi.org/10.1007/s10236-005-0024-3. Available at.
Zhang, C., Li, C., 2019. Effects of hurricane forward speed and approach angle on storm surges: an idealized numerical experiment. Acta Oceanologica Sinica 38 (7), 48–56. https://doi.org/10.1007/s13131-018-1081-z. Available at.
Zhang, X., Marta-Almeida, M., Hetland, R.D., 2012. A high-resolution pre-operational forecast model of circulation on the Texas-Louisiana continental shelf and slope. J. Oper. Ocean. 5 (1), 19–34. https://doi.org/10.1080/1755876X.2012.11020129. Available at.
Zhong, L., Li, M., Zhang, D.L., 2010. How do uncertainties in hurricane model forecasts affect storm surge predictions in a semi-enclosed bay? Estuar. Coast. Shelf. Sci. 90 (2), 61–72. https://doi.org/10.1016/j.ecss.2010.07.001. Available at.